EFFECTS OF SOLIDIFICATION VARIABLES ON INGOT STRUCTURE

by

M. C. Flemings
T. F. Bower
T. Z. Kattamis
H. D. Brody

Casting and Solidification Section
Department of Metallurgy
Massachusetts Institute of Technology
Cambridge, Massachusetts

Prepared Under Contract No.
DA-19-020-ORD-5706(A)
(June 1964 - June 1965)

For

Department of Army, Materiel Command, MUCOM,
Frankford Arsenal, Philadelphia, Pa. 19137

(EFFECTS OF SOLIDIFICATION VARIABLES ON INGOT STRUCTURE)

by

M. C. Flemings
T. F. Bower
T. Z. Kattamis
H. D. Brody

Casting and Solidification Section
Department of Metallurgy
5 Massachusetts Institute of Technology
6 Cambridge, Massachusetts

Prepared Under Contract No.

DA-19-020-ORD-5706(A) 13

9 (June 1964 - June 1965)

For

12
Department of Army, Materiel Command, MUCOM,
Frankford Arsenal, Philadelphia, Pa. 19137

⑩
Publication Date: May 1, 1966

start

ABSTRACT

Results are summarized of experimental and analytical studies of solutionizing aluminum alloys containing a non-equilibrium second phase. Dendrite arm spacing, solution treatment temperature, and alloy content are the important processing variables determining time required to eliminate second phase. At a typical temperature used to solutionize "premium quality" aluminum-4.5 per cent copper alloy castings, required time for essentially complete elimination of second phase is 25 times the original solidification time.

The classical explanation for formation of the fine equiaxed "chill zone" in ingot solidification is that local supercooling near the chill wall causes copious nucleation in this region. Work reported herein indicates, however, that convection is an essential element in formation of the chill zone. In the absence of convection, no chill zone forms even though rate of heat extraction is extremely rapid. Alloy studied was al aluminum-4.5 per cent copper alloy solidified against a copper chill wall. When solidification was initiated at the chill wall in absence of convection, surface grain size was large (>1 cm diameter). When it was initiated in the presence of convection, it was fine (<0.5 cm diameter).

al

A study was conducted of the dendritic structure of the surface grains described above. The structure is readily apparent, without polishing or etching. Most primary and secondary "arms" in the surface dendrite structure are arranged orthogonally, giving the impression of strong preferred orientation on the surface. However, no such preferred orientation exists and it is therefore evident the "arms" do not represent <100> directions.

The primary "arms" are shown to be intersections of a {100} plane with the chill plane, or, more rarely, the projection of a <100> direction on the chill plane. Traces of secondary dendrite "arms" are usually within a few degrees of 90° to the primary trace independence of dendrite orientation. Primary, secondary and higher order dendrite traces almost always represent intersections of {100} planes with the chill surface, or projections of <100> directions.

Dendrite traces are often observed to be bent. In these cases the crystal lattice changes orientation; bending is concave to the chill surface.

Experiments were conducted on dendritic and non-dendritic solidification of aluminum-copper alloys and of a magnesium-zinc alloy. Grain diameter in the non-dendritic melts was found to depend on solidification time in quantitatively the same way as dendrite arm spacing in the dendritic melts.

do ii

An explanation of the above results is given based on structure coarsening ("ripening") during solidification. It is concluded that "dendrite element spacing" (arm spacing in the dendritic melts, grain diameter in the non-dendritic melts) is determined not by how many elements form during initial growth, but rather by how many such elements disappear by ripening during growth.

Microsegregation (as measured by amount of second phase) is shown to be substantially less in the non-dendritic aluminum and magnesium base alloys than in the comparable dendritic alloys.

Experimental data on dendrite arm spacings in aluminum-copper alloys are compared with an analysis based on coarsening kinetics. Arm spacings are shown to depend on the quantity $\bar{M}t_f$ ($\bar{M}$ = coarsening parameter, t_f = solidification time) for a wide range of alloy analyses and solidification times. The engineering importance of the agreement found is that for the first time:

(1) It appears the mechanism controlling final dendrite arm spacings in castings and ingots has been established.

(2) It should be possible to correlate experimental measurements on dendrite arm spacings from different alloys and different alloy systems.

(3) It should be possible to predict at least semiquantitatively the influence of alloy variables or other process variables on dendrite arm spacing.

end

TABLE OF CONTENTS

Start

Chapter 1: INTRODUCTION

This report summarizes a part of a continuing research program on casting and ingot solidification of aluminum base alloys; earlier phases of the work have been reported[1-6].

Chapter 2 presents experimental and analytical work on solution treatment. This work was undertaken because previous studies have shown that mechanical properties of both cast and wrought aluminum alloys are strongly dependent on degree of homogeneity obtained in the solution treatment[7-9]. The previous studies have also shown it is extremely difficult to obtain a high degree of homogeneity in most such alloys. A detailed understanding of the kinetics of solutionizing aluminum alloys is therefore of considerable engineering importance.

One of the important factors promoting rapid solutionizing is a fine dendrite arm spacing, achieved by rapid solidification. Considerable attention has therefore been paid to rapidly solidified structures in this report, as well as in earlier phases of the research[2,6]. Chapters 3 and 4 deal with the details of the grain and dendrite structures in the surface grains, immediately adjacent the chill; several rather unexpected conclusions are reached.

In the last annual report[2], some attention was paid to a technique of achieving "non-dendritic" solidification in an aluminum alloy. Some further experiments are reported in Chapter 5 on the technique, and some experiments on "non-dendritic" solidification of a magnesium-zinc alloy are included. These experiments, together with those of a separate research program on undercooled structures, have led to the surprising conclusion that dendrite arm spacing is determined by "ripening" kinetics, not by growth instabilities.

Some experiments, reported in Chapter 5, were conducted to verify this conclusion. An analysis of ripening kinetics is then presented and an attempt made to predict dendrite arm spacings in different aluminum alloys on the basis of ripening kinetics. It is concluded that the analysis presented should prove to be a tool of considerable engineering value.

Research summarized in Chapter 2 was conducted by Dr. H. D. Brody and Dr. B. P. Bardes. Chapters 3 and 4 comprise work of Dr. T. F. Bower. Chapter 5 describes research of Mr. U. T. Holmberg, and Chapter 6 is work of Dr. T. Z. Kattamis and Mr. J. Coughlin.

REFERENCES

1. H. D. Brody and M. C. Flemings, "Investigation of Parameters Influencing Solidification Behavior of Aluminum Alloys", Annual Report, Contract No. DA-19-020-ORD-5706(A), (June 1962 - June 1963) to Army Material Command, Frankford Arsenal.

2. T. F. Bower, H. D. Brody and M. C. Flemings, "Effects of Solidification Variables on the Structures of Aluminum Base Ingots", Annual Report Contract No. DA-19-020-ORD-5706(A), (June 1963 - June 1964) to Army Material Command, Frankford Arsenal.

3. H. D. Brody and M. C. Flemings, "Solute Redistribution in Dendritic Solidification", accepted for publication, Trans. Met. Soc. A.I.M.E.

4. T. F. Bower, H. D. Brody and M. C. Flemings, "Measurements of Solute Redistribution in Dendritic Solidification", accepted for publication, Trans. Met. Soc. A.I.M.E.

5. T. S. Piwonka and M. C. Flemings, "Pore Formation in Solidification", accepted for publication, Trans. Met. Soc. A.I.M.E.

6. B. Bardes and M. C. Flemings, "Dendrite Arm Spacing and Solidification Time", accepted for publication, Trans. A.F.S., 1966.

7. E. M. Passmore, M. C. Flemings and H. F. Taylor, "Fundamental Studies on Effects of Solution Treatment, Iron Content, and Chilling of Sand Cast Aluminum-Copper Alloy", Trans. A.F.S., v. 66, 1958, pp. 96 - 104.

8. M. C. Flemings, "Controlled Solidification", Proceedings Twelfth Sagamore Army Materials Research Conference, August, 1963.

9. S. Lipson, H. Antes, and H. Rosenthal, unpublished work, Frankford Arsenal.

Chapter 2: SOLUTION TREATMENT

A. Introduction

High strength aluminum casting alloys require solution treatment to develop high mechanical properties. It has been shown that usual commercial solution treatments do not, in general, fully solutionize the structure and that treatments at higher temperatures, and for longer times, than those usually employed result in substantially improved mechanical properties[1,2].

It is now becoming evident that much the same can be said of wrought material. Ingot soaking treatments, and combined thermo-mechanical treatments during working do not fully homogenize high strength wrought alloys. Substantial improvements in ductility can be obtained in these alloys (e.g., the 7000 series) by processing treatments which fully homogenize the structure. Moreover, these processing treatments permit increasing the solute content, and thereby the strength as well as ductility, to levels well above those of current commercial alloys[3].

For the foregoing reasons, detailed understanding of the solutionizing process, and of methods of accelerating its rate would be of great value. The following portion of this research was undertaken with these aims in mind.

B. Analyses and Computations

Solution (homogenization) treatments seek to reduce or eliminate microsegregation resulting from non-equilibrium solidification. This solidification segregation occurs over the scale of the dendrite spacing and requires much longer times to eliminate than that resulting from solid state phase changes. Macrosegregation, in general, is not removed by solution treatment.

Most aluminum alloys solidify with the formation of a second phase. Alloys lower in solute content than the maximum solubility limit are, ideally, solution treated to form a single phase alloy. Alloys higher in solute content than the solubility limit are, ideally, solution treated to achieve the maximum concentration of solute in the primary phase; i.e., to form the equilibrium ratio of phases. Alloys that have complete solid solubility solidify with a non-uniform distribution of solute in the single solid phase. For these alloys to respond uniformly to further heat treatment, they are, ideally, solution treated to eliminate significant gradients within the dendrites.

In the following analysis of solute treatment, the rate limiting factor is taken to be the ability of the dendrites to accommodate solute from the unstable secondary phases; and in single phase alloys, the rate of diffusion within the dendrites. The analysis is based on a finite difference solution to Fick's second law for diffusion assuming a pre-solution treatment solute distribution in the dendrites based on previously reported analyses[4-7].

The computation is effected by assuming the alloys to be held at a certain temperature, T, and allowing diffusion to take place within the primary solid for a short interval of time Δt, with a computed diffusion coefficient, $D_S = f(T)$. The increase of solute content within the primary phase is then computed and an equivalent amount of eutectic phase caused to "dissolve".

Initial Conditions.

The model employed for computations is described in earlier reports and papers[4-7]. Dendrites are idealized as simple plates whose spacing is small with respect to the mushy zone. Solute distribution across the plate thickness resulting from the initial, relatively rapid cooling of the alloy from the liquidus to room temperature is computed by a numerical analysis technique. The limited diffusion of the solute within the solid phase is taken into account: calculations are made for a particular dendrite spacing, (2ℓ), and solidification time, θ_f.

The composition distribution resulting from the solidification calculation is used as the initial solute distribution in the homogenization treatment; both calculations for a particular alloy are based on the same value of ℓ, (where ℓ is half the dendrite spacing) and θ_f.

Method of Computation.

The solute balance is shown schematically in Figure 1; where X_i is the position of the interface, C_E is the average composition of the eutectic phase, C_S^* is the solute content in the primary solid at the interface, and line A indicates the distribution of solute within the primary phase at time t. The boundary conditions are

$$\frac{\partial C_S}{\partial X} = 0, \text{ at } X = 0; \quad C_S = C_S^* \text{ (max. solubility)} \quad \text{at } X = X_i \tag{1}$$

where X_i, the position of the interface, is continually increasing as homogenization proceeds.

Diffusion within the primary phase is computed by considering the solid to be divided into several slabs each ΔX in thickness. The composition within one slab after diffusion is allowed to proceed for a time $\Delta t \approx \frac{\Delta X^2}{2D_S}$ is, by the finite difference method[8],

$$C_{S_{j,k}} = \frac{C_{S_{j-1,k-1}} + (M - 2)\, C_{S_{j,k-1}} + C_{S_{j+1,k-1}}}{M} \tag{2a}$$

where

$$M = \frac{\Delta X^2}{D_S \Delta t} \tag{2b}$$

and the subscripts j refers to the position of the slab in relation to the centerline and k refers to increments of time (k-1 is at time t, k at time t + Δt). The solute distribution at time t + Δt is computed by iteratively evaluating (2) from the slab at the centerline ($J = 1$) to the slab adjacent the interface ($J = [X_i + \Delta X]/\Delta X$). The interface during this part of the computation remains stationary and at the equilibrium composition C^*_S. The new solute composition within the primary phase is indicated in Figure 1 by line A'.

Then the total amount of solute that entered the primary dendrite during Δt, shaded area of solid phase in Figure 1, is computed and an equivalent amount of solute is considered to be removed from the eutectic. The interface is moved ahead an increment, ε, proportional to the amount of eutectic removed during Δt. If Ω is the new solute in the primary phase, then

$$\varepsilon = \frac{\Omega}{C^*_L - C^*_S} \cdot \ell \qquad (3)$$

Diffusion within the primary dendrite is computed for another Δt, and the procedure continues until the primary dendrites impinge at $X = \ell$ or until an equilibrium ratio of phases is reached.

When no second phase is present but a non-uniform single phase solid is to be homogenized, the boundary conditions are

$$\frac{\partial C_S}{\partial X} = 0, \text{ at } X = 0; \quad \frac{\partial C_S}{\partial X} = 0, \text{ at } X = \ell \qquad (4)$$

and again the amount of diffusion is computed by the finite different solution of Fick's second law, now using (4) for the boundary conditions.

C. Quantitative Results: Homogenization Treatments

The time to completely eliminate the second phase by solutionizing an aluminum-4.5 per cent copper alloy was computed for a variety of conditions that represent a wide range of casting practice. The results are summarized by Figures 2 to 7.

The distribution of solute in the primary phase, κ, is shown in Figure 2 at successive stages during solution treatment of aluminum-4.5 per cent copper alloy at 548°C (i.e., just below the eutectic temperature) for a value of $\eta = 1 \times 10^8$ (where $\eta = \theta_f/\ell^2$). The lowest curve depicts the solute distribution immediately after solidification at time θ_f (where the symbol θ is used to denote time from the beginning of solidification and t is used to denote time from the beginning of solution treatment. Thus, $\theta = t + \theta_f$.) During the isothermal hold, the solute content at each point within the primary solid approaches the average alloy composition, $C_0 = 4.5$ per cent copper, and the interface between primary and eutectic phases advances in the direction of the eutectic. At time θ_6 the eutectic is eliminated and the average composition of the solid is 4.5 per cent. The copper content varies across the dendrite from 3.85 to 5.64 per cent.

The computed average composition of the alloy after homogenization will differ, for some values of η from the original solute content due to the approximate nature of the initial solidification model. Refining the analysis to satisfy exactly the material balance would alter only slightly the calculated results for aluminum-copper alloys (and such a refinement is not justified by the available data).

The advance of the solid-liquid interface is depicted by Figure 3 for heat treatments of aluminum-4.5 per cent copper alloy at several temperatures in the solutionizing range. The weight fraction of non-equilibrium phase corresponding to the interface position is indicated on the right ordinate axis. Note that the time to eliminate the θ phase quickly increases with decreasing temperature; i.e., as the diffusion coefficient diminishes. In Figure 3, the decrease in the rate of advance of the interface is apparent at the end of solutionizing, when the concentration gradients approach zero.

For a given alloy with a given solidification structure characterized by η, one homogenization curve can be drawn for all temperatures within the solutionizing range by plotting some measure of segregation versus the dimensionless factor $D_S t/\ell^2$, where D_S is the solute diffusion coefficient, t is the time the structure has been at the homogenization temperature; and ℓ is a characteristic spacing, such as one half the dendrite spacing. The temperature dependence*

---

* The boundary conditions for the analysis of solution treatment, condition (1), fix the solute content in the primary solid at the interface at the solubility limit; i.e., the solvus is considered a vertical line. If the second phase (in aluminum-4.5 per cent copper alloy, the θ phase) does not have difficulty nucleating and the primary and secondary phases can adjust their proportions and their compositions to satisfy equilibrium locally, homogenization kinetics will not differ significantly from the analysis (for systems with gradually sloping solvus lines).

is incorporated in D_S and the structure dependence in ℓ^2.

The "segregation ratio", S, of a solute element distributed in a dendritic structure, may be defined as

$$S = \frac{C_M}{C_m} \qquad (5)$$

where C_M is the maximum solute concentration of the primary solid phase and C_m is the minimum solute concentration. For calculation of homogenization kinetics, it is useful to define an "index of residual segregation", δ_S, as

$$\delta_S = \frac{C_M - C_m}{C_M^\circ - C_m^\circ} = \frac{S - 1}{S^\circ - 1} \; \frac{C_m}{C_m^\circ} \qquad (6)$$

where the superscript ° refers to the as-cast structure. The index of residual segregation will be unity for the as-cast structure and will be zero when the primary solid phase has a uniform composition. In Figure 4, δ_S is plotted versus the dimensionless parameter $D_S t/\ell^2$ for aluminum-4.5 per cent copper alloy with $\eta = 2 \times 10^7$ sec/cm^2. Similar curves would be obtained for other values of η.

In Figure 5, the solutionizing time required for elimination of eutectic (at just under the eutectic temperature) is given as a function of half the dendrite arm spacing, ℓ. Note that the value of η chosen to describe the original segregation has little effect on this time; the solutionizing time is much more dependent on dendrite arm spacing than on extent of diffusion during solidification, or during subsequent cooling to room temperature.

As long as the dendrite spacing is proportional to the square root of solidification time, i.e., as long as η is a constant, homogenization times will increase in proportion to the solidification time. For example, a casting that solidified in one half hour would take sixty times as long to homogenize as one solidified in thirty seconds. For aluminum-copper alloys, η increases as the solidification time increases, and thus, the extent of segregation in the as-cast structure becomes less[4-7]. In Figure 6, the homogenization time predicted for aluminum-4.5 per cent copper alloy, is plotted on log scale as a function of solidification time, based on dendrite spacing measurements of Michael and Bever[9]. A line of slope one is drawn to indicate the advantage due to solid diffusion during solidification.

For comparison with experimental data (to be discussed below), Figure 7 shows results of the computer program, plotted in a slightly different way, and for aluminum-4.65 per cent copper alloy. The figure shows how the amount of non-equilibrium phase ($CuAl_2$) is expected to vary with η and relative homogenization time t/θ_f at 535°C. For a typical value of η for this alloy, 4×10^8 sec/cm^2, predicted solutionizing time for elimination of eutectic is about ten times solidification time. A similar conclusion is reached by examination of earlier figures (e.g., Figure 5).

Measurements made on samples homogenized at 535°C can be plotted directly on Figure 7. Measurements made at other homogenization temperatures, T, can be compared to theory by multiplying the measured homogenization time by the factor $D_S(535)/D_S(T)$. (The same assumptions which are made on page 9 (footnote), must be made here.)

D. Experiments

In this work homogenization of a columnar water cooled ingot was studied. Methods of casting the ingot, measuring solidification times and measuring dendrite spacings were reported previously[5]. Specimens were taken from 1, 3, and 5 inch levels of the ingot. Small pieces about 3 x 3 x 3 millimeters were held at 535°C or 545°C for 0, 12, 25, 50, 100, 250, 500, 1050, and 2600 minutes. The small size of the specimen insured rapid and uniform heating and cooling. Quantitative metallography was used to follow dissolution of non-equilibrium eutectic material.

Two types of intermetallic compound were observed in these specimens. They were identified to be $CuAl_2$ and Cu_2FeAl_7. The latter particles were similar in shape and etching behavior to particles identified by Passmore et al[2] as Cu_2FeAl_7. Scanning X-ray analysis of one of these particles indicated a ternary intermetallic rich in iron and copper. The ternary equilibrium diagram given by Phillips[10] indicates that an alloy containing 4.65 per cent copper and 0.06 per cent iron would contain approximately 0.33 weight per cent of the ternary intermetallic at equilibrium at 535°C.

Quantitative metallography was conducted using procedures outlined by Cahn[11]. A grid of 49 regularly spaced points was superimposed upon the field of view of a metallograph. The number of points of the grid falling over each of the two intermetallic phases was determined for each of 200 random placements of the grid over the specimen. The fraction of the 9800 points falling over each phase represented the volume fraction of that phase in the alloy. To resolve the regions of eutectic into the three phases present ($CuAl_2$, Cu_2FeAl_7 and the aluminum-rich solid solution) the work was done at a magnification of 1000X. Hilliard and Cahn[12] have estimated the statistical standard deviations for a number of methods of volume-fraction analysis; the standard deviation for these measurements is less than 3 per cent of the reported value.

Measurements of the volume fraction $CuAl_2$ were converted to weight fractions using the value of the density of $CuAl_2$ of 4.40 g/cc reported by Michael and Bever[9]. These data are reported in Table 1 and Figure 7. The data for the as-cast conditions are shown at relative homogenization time of 0.1; this is an approximation designed to place the as-cast ingots on the same graph as the homogenization specimens. The density of the Cu_2FeAl_7 phase was calculated from the lattice parameter data given by Smithells[13] and the atomic weights of the elements present; the value obtained was 4.22 g/cc. The as-cast specimens contained about 2.25 per cent $CuAl_2$ and 0.30 per cent Cu_2FeAl_7. The amount of Cu_2FeAl_7 corresponds quite closely to the value of 0.33 per cent obtained from the wet analyzed composition and the equilibrium diagram. In addition to the amounts of $CuAl_2$ reported in Table 1 and Figure 7 every homogenized specimen contained 0.30 per cent Cu_2FeAl_7.

E. Interpretation of Experiments

In agreement with theory, data in Figure 7 corresponds approximately to the theoretical curve for $\eta = 4 \times 10^{+8}$, during the early stages of solution treatment. However, elimination of the last of the second phase requires a substantially longer time than that predicted for this value of η. Theory indicates, as noted above, that all second phase should be eliminated for $t/\theta_f \simeq 10$ and, indeed, marked reduction of second phase is obtained in this time. However, for its essentially complete elimination t/θ_f must be considerably larger, approximately 25.

The explanation for this deviation from theory lies, almost certainly, primarily in the fact that dendrites are not simple plates, but are rather complex structures with small composition perturbations over distances the order of the secondary and tertiary arm spacing and larger perturbations over primary arm spacings[7]. Hence it is to be expected that in the initial stages of solutionizing, diffusion need occur only over tertiary or secondary arm spacings; however, the last of the second phase can presumably be eliminated only by diffusion over the primary arm spacing. Hence, the effective η describing the diffusion is expected to decrease as amount of second phase decreases. In Figure 7 this is evidently the case. Data agree with theory in initial stages of homogenization of $\eta \approx 4 \times 10^{+8}$ sec/cm^2; in late stages of homogenization agreement requires $\eta \approx 8 \times 10^7$ sec/cm^2.

Figure 8 shows this change in required diffusion distance metallographically, using a "differential precipitation" technique. Samples studied were deliberately overaged by holding at 405°C for 4.25 hours. Since the solubility of copper at 405°C is approximately 1.5 per cent copper, precipitate particles would be expected to form in all regions richer in copper. Thus the boundaries of precipitate free regions as revealed by etching should be, ideally, isoconcentration contours of 1.5 per cent copper. In fact, comparison of metallographic results with those of electron microprobe measurements indicated that an isoconcentration contour was delineated by the boundary of precipitate region, but that this boundary was richer in solute than that predicted by the equilibrium diagram (for the 405°C treatment noted above the boundary was at 2.85 per cent copper). Section a, b, c, d in this figure show the etched structure at values of t/θ_f of, respectively, 0, 1.33, 2.78, and 5.56. Note that concentration differences on the fine scale of the order of secondary arms are gradually obliterated during heat treatment until, at $t/\theta_f = 5.56$ regions having compositions less than 2.85 per cent copper exist only at primary arms. Final, complete homogenization must clearly involve diffusion over distances the order of this spacing.

As noted above, essentially complete elimination of second phase was found in this work to occur in solution treatments at 535°C (995°F) in times the order of 25 times the solidification time. As numerical illustration, using data on solidification times reported in the previous Annual Report[5], this requires a homogenization time of 1.7 hours for a location on a water cooled unidirectional ingot 1 inch from the chill and 6 hours for a location 5 inches from the chill.

Data reported by Passmore, Flemings, and Taylor[2] (on mechanical properties of this alloy after various solution treatments) shows that the major property improvements effected by solutionizing occur within the times calculated above. However, these data also show some continuing property improvement after longer solution times at higher temperatures, presumably because of elimination of remaining traces of second phase and/or further reduction of coring in the primary phase.

F. Conclusions

The plate-like dendrite model described in detail earlier has been employed to obtain an understanding of the kinetics of solutionizing of aluminum alloys containing a non-equilibrium second phase. For a given alloy, dendrite arm spacing and homogenization temperature are the important parameters affecting time required to eliminate the second phase. Extent of diffusion in the solid during solidification is of secondary importance.

For aluminum-4.5 per cent copper solution treated just under the eutectic temperature, the analysis predicts that homogenization time must be approximately 7 times the solidification time. At 535°C (the highest temperature ordinarily used to heat treat "premium quality castings" of this alloy) approximately 10 times the solidification time is predicted. At 517°C (a typical temperature for commerical solution treating of this alloy) approximately 15 times solidification time is predicted.

The foregoing predictions are based on a value of η determined for the alloy from earlier studies, using an analysis based on plate-like dendrite arms. Metallography, however, shows the dendrite structure is considerably more complex than simple plates and that required diffusion distance increases with decreasing residual second phase.

Experiments reported herein on residual second phase after solutionizing show general agreement with theory for $\eta = 4 \times 10^{+8}$ sec/cm^2 for early stages of homogenization. In later stages, deviation results from the longer required diffusion path and required homogenization times to eliminate second phase are approximately 2-1/2 times those calculated. For example, at a typical temperature used to solutionize "premium quality" castings of this alloy (535°C, 995°F), required time for essentially complete elimination of second phase (as determined experimentally) is approximately 25 times solidification time. Elmination of coring in the primary phase requires much longer times.

REFERENCES

1. "Parameters for Controlled Solidification in Aluminum Castings", Final Report, Foundry Section, Department of Metallurgy, Massachusetts Institute of Technology, Frankford Arsenal DA-19-020-ORD-3674, July, 1957.

2. E. M. Passmore, M. C. Flemings, H. F. Taylor, "Fundamental Studies on Effects of Solution Treatment, Iron Content, and Chilling of Cast Aluminum-Copper Alloy", Trans. A.F.S., Vol. 66, 1958.

3. H. Antes, S. Lipson, H. Rosenthal, Unpublished work, Frankford Arsenal, Philadelphia, Pennsylvania.

4. H. D. Brody, M. C. Flemings, "Investigation of Parameters Influencing Solidification Behavior of Aluminum Alloys", Annual Report, Massachusetts Institute of Technology, Army Materials Research Agency, Contract No. DA-19-020-ORD-5706(A), Frankford Arsenal, Philadelphia, Pennsylvania, July, 1963.

5. T. F. Bower, H. D. Brody, M. C. Flemings, "Effects of Solidification Variables on the Structure of Aluminum Base Ingots", Annual Report, Massachusetts Institute of Technology, Army Materials Research Agency, Contract No. DA-19-020-ORD-5706(A), Frankford Arsenal, Philadelphia, Pennsylvania, July, 1964.

6. H. D. Brody, M. C. Flemings, "Analysis of Microsegregation in Dendritic Solidification", accepted for publication, Trans. Met. Soc., A.I.M.E., 1966.

7. T. F. Bower, H. D. Brody, M. C. Flemings, "Measurement of Microsegregation in Dendritic Solidification", accepted for publication, Trans. Met. Soc., A.I.M.E., 1966.

8. H. S. Carslaw, J. C. Jaeger, <u>Conduction of Heat in Solids</u>, 2nd ed., Clarendon Press, Oxford, 1959.

9. A. B. Michael, M. B. Bever, "Solidification of Aluminum Rich Aluminum-Copper Alloys", Trans. A.I.M.E., Vol. 200, 1954.

10. H. W. L. Phillips, <u>Annotated Equilibrium Diagrams for Some Aluminum Alloy Systems</u>, Institute of Metals, London, 1959.

11. J. W. Cahn, Professor of Metallurgy, Massachusetts Institute of Technology, private communication.

12. J. E. Hilliard, J. W. Cahn, "An Evaluation of Procedures in Quantitative Metallography for Volume Fraction Analysis", Trans. A.I.M.E., Vol. 221, 1961, pp. 344-352.

13. C. J. Smithells, <u>Metal Reference Book</u>, Vol. 2, 3rd ed., Butterworth's, Washington, 1962.

TABLE 1

HOMOGENIZATION TIMES AND AMOUNTS OF RESIDUAL $CuAl_2$

Homogenization time (minutes)	Relative homogenization time (at 535°C)	Weight per cent $CuAl_2$
One inch from chill, heat treated at 545°C.		
0	0	2.59
12	2.30	1.63
25	4.79	0.89
50	9.58	0.35
100	19.17	0.061
Three inches from chill, heat treated at 535°C		
0	0	2.25
12	1.33	2.02
25	2.78	1.47
50	5.56	1.05
100	11.11	0.51
150	16.67	0.20
Three inches from chill, heat treated at 545°C		
0	0	2.25
12	1.53	1.97
25	3.19	1.32
50	6.38	0.68
100	12.77	0.25
Five inches from chill, heat treated at 545°C		
0	0	2.63
12	0.92	2.27
25	1.91	2.14
50	3.83	1.15
100	7.67	0.79
250	19.14	0.38

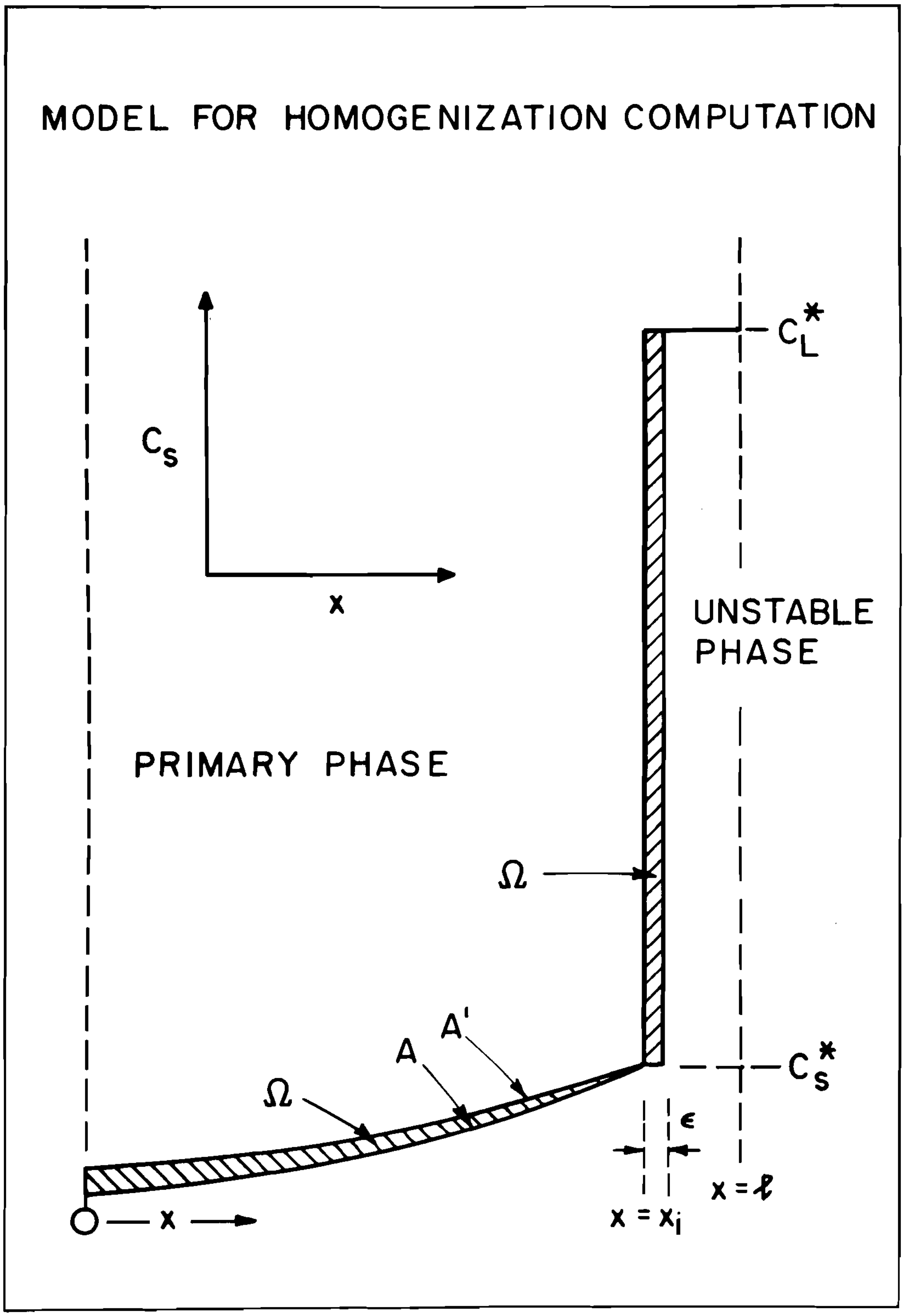

Figure 1: Schematic representation of model for homogenization computations.

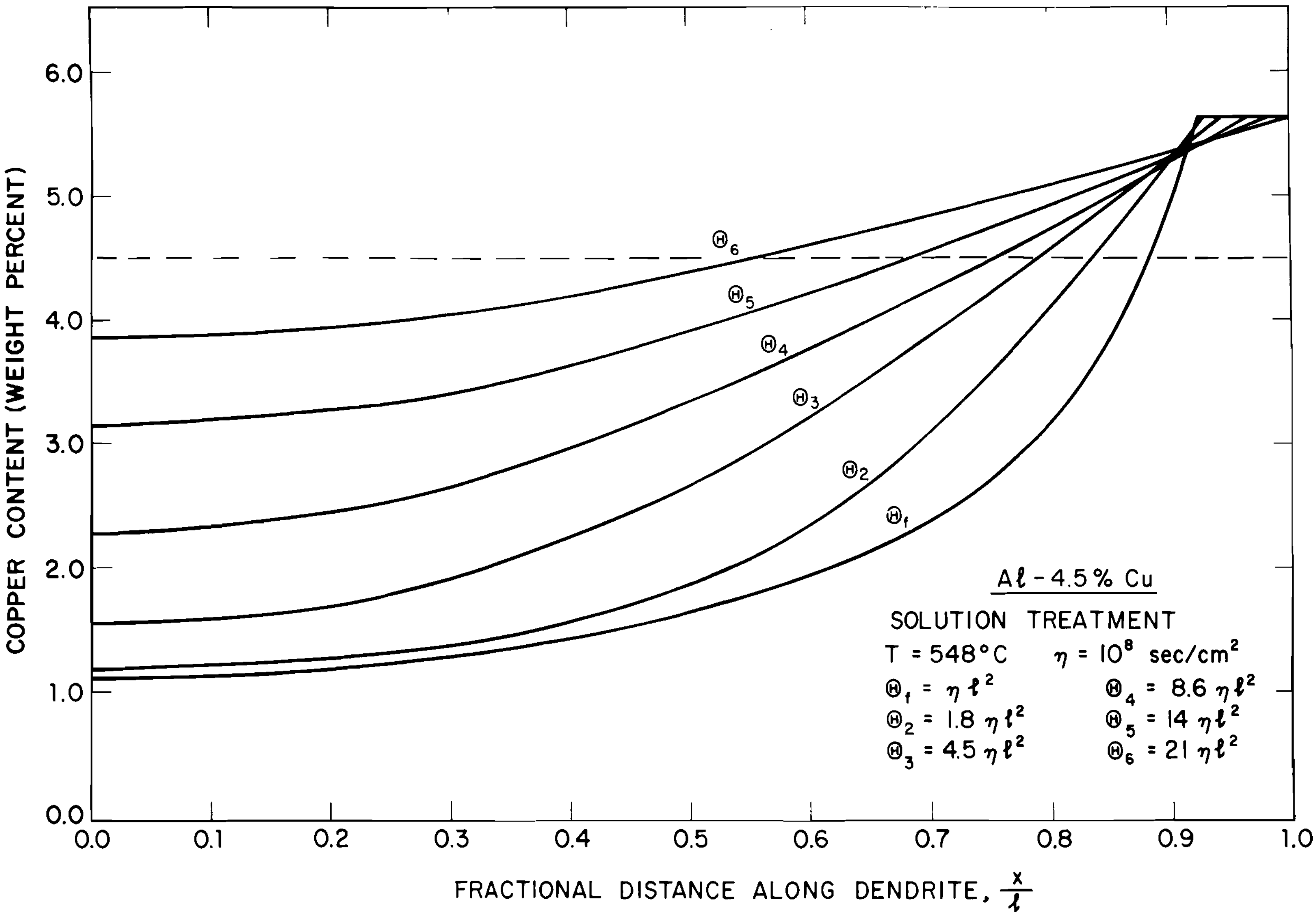

Figure 2: Solute distribution in primary phase at successive stages in the solution treatment of an aluminum-4.5 per cent copper alloy.

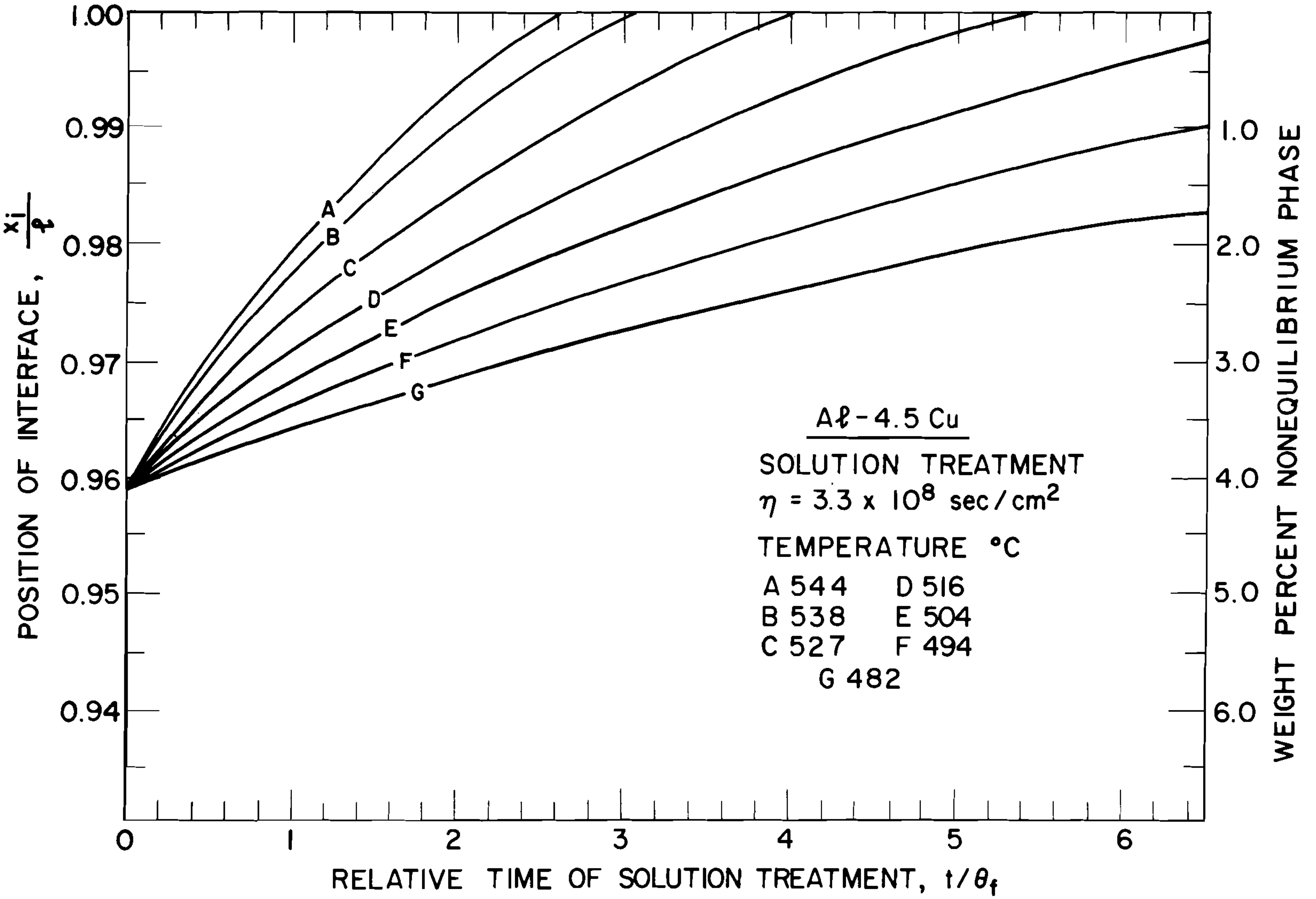

Figure 3: Position of the interface during isothermal heat treatment of aluminum-4.5 per cent copper alloy at several temperatures.

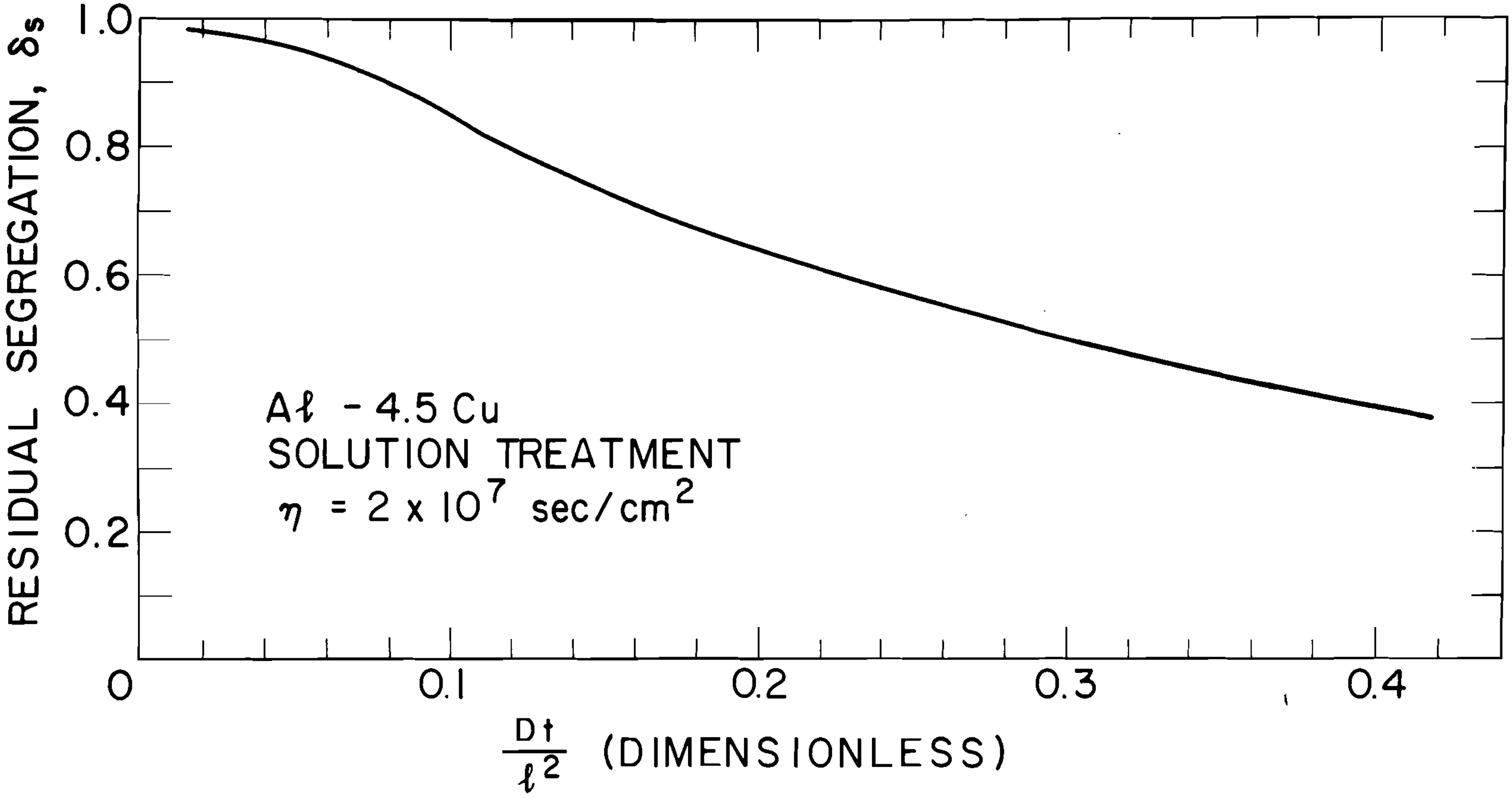

Figure 4: The index of residual segregation, δ_S, during solution treatment of an aluminum-4.5 per cent copper alloy plotted versus the dimensionless parameter Dt/ℓ^2.

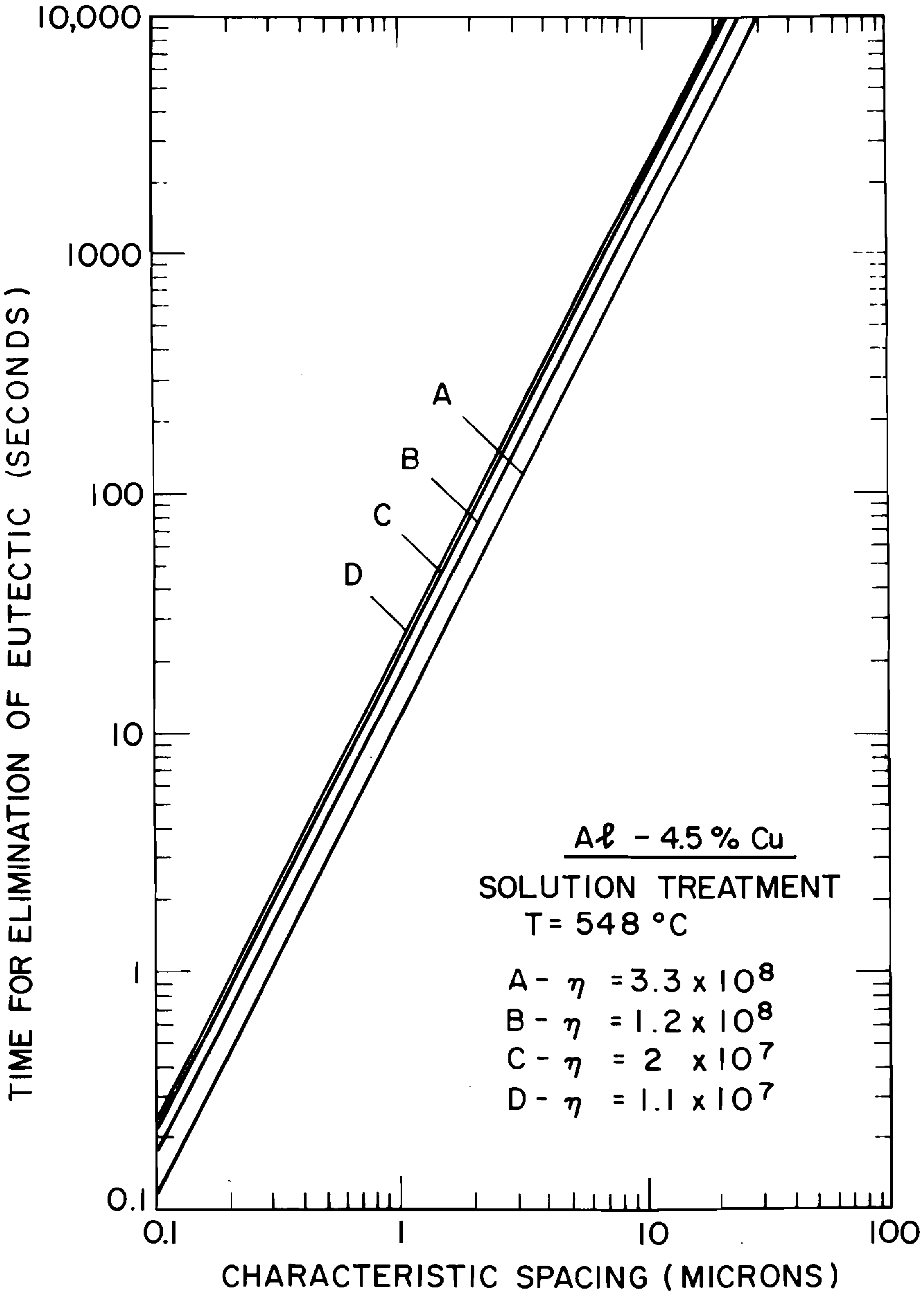

Figure 5: Time to eliminate the non-equilibrium phase in an aluminum-4.5 per cent copper alloy by solution treatment at 548°C plotted versus the characteristic spacing, ℓ (logarithmic scales).

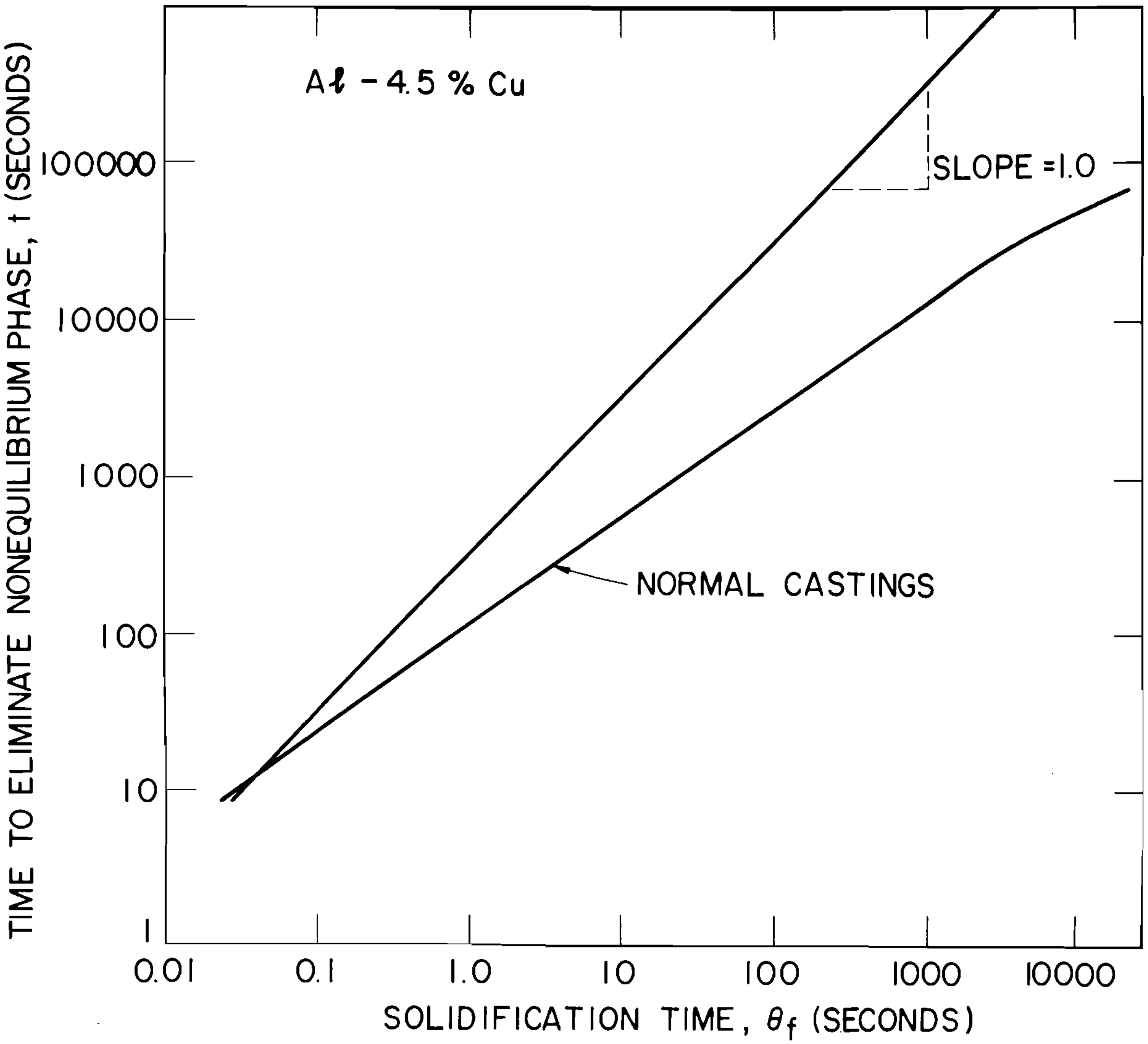

Figure 6: Time to eliminate the non-equilibrium phase in aluminum-4.5 per cent copper alloy in normal castings heat treated at 548°C (using dendrite measurements of Michael and Bever[9]).

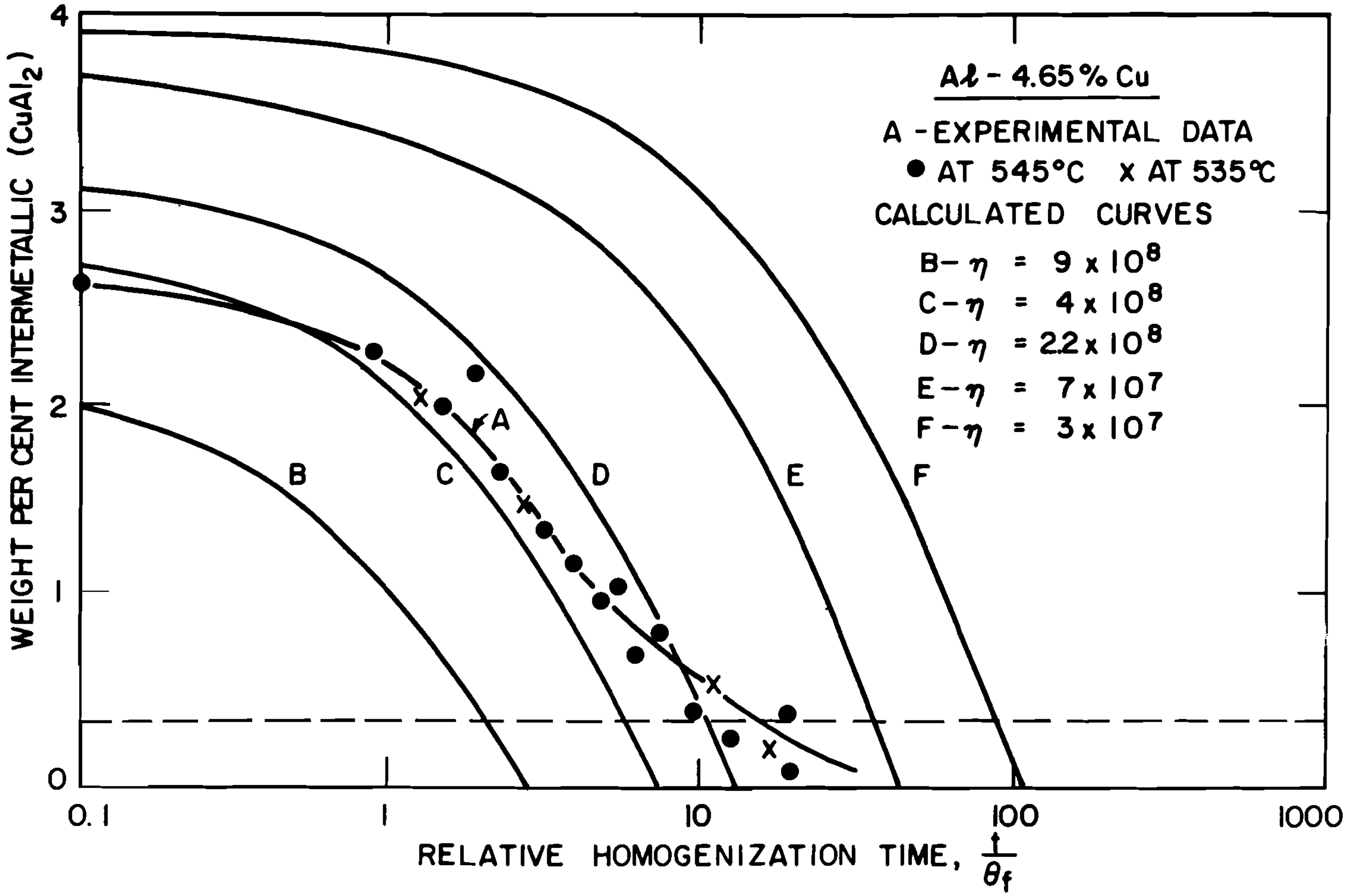

Figure 7: Solid curves B-F are results of computer calculations of homogenization of aluminum 4.65 percent copper alloy, at 535°C.

Crosses and circles show experimental points for homogenization at 535°C and 545°C, respectively, adjusted for equivalent homogenization time at 535°C. Dotted line shows amount of Cu_2FeAl_7 present (in addition to $CuAl_2$).

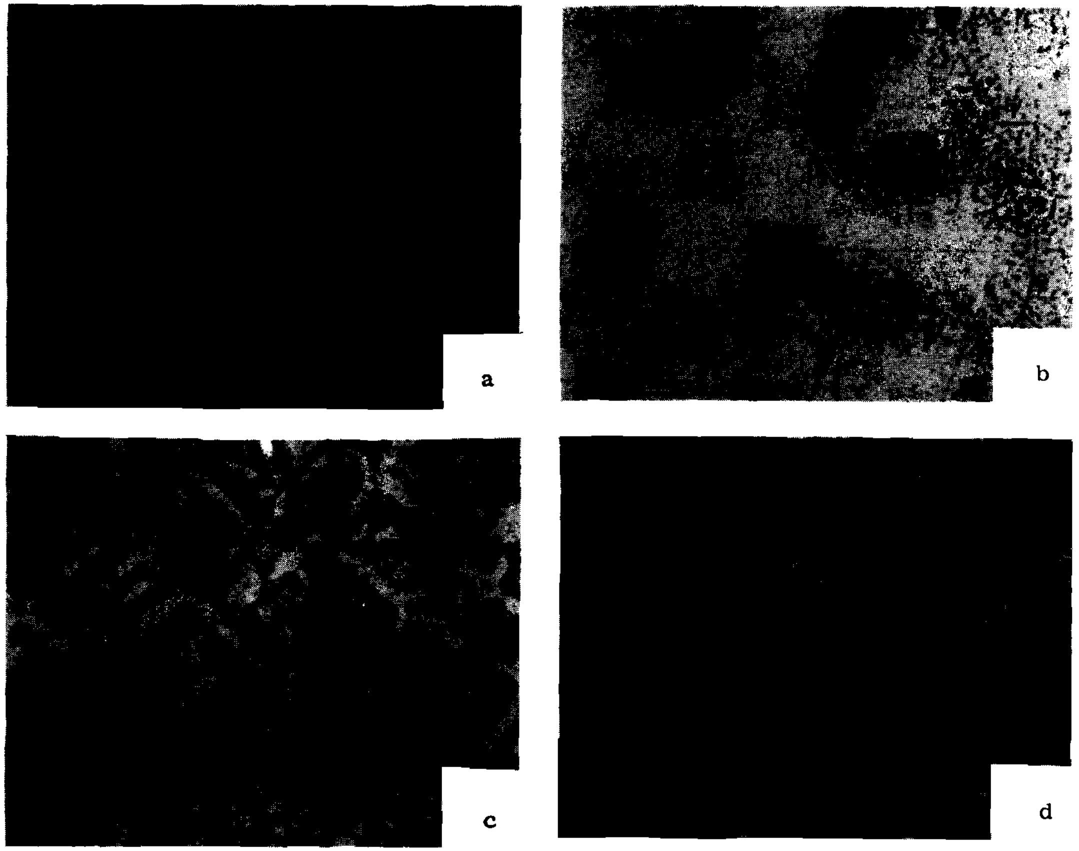

Figure 8: Sample three inches from chill in unidirectionally solidified ingot, (a) as-cast and with relative homogenization times of (b) 1.33, (c) 2.78, and (d) 5.56. Samples have been given differential precipitation treatment at 405°C to show 2.85 per cent copper isoconcentration contour. (Etch: 25 ml HNO_3, 0.5 ml HF, 10 g $Fe(NO_3)_3$, 75 ml H_2O. Magnification, 50X.)

Chapter 3: FORMATION OF THE CHILL ZONE IN INGOT SOLIDIFICATION

ABSTRACT

The classical explanation for formation of the fine equiaxed "chill zone" in ingot solidification is that local supercooling near the chill wall causes copious nucleation in this region. This work indicates, however, that convection is an essential element in formation of the chill zone. In the absence of convection, no chill zone forms even though rate of heat extraction is extremely rapid.

Alloy studied was aluminum-4.5 per cent copper alloy solidified against a copper chill wall. When solidification was initiated at the chill wall in absence of convection, surface grain size was large (>1 cm. dia.). When it was initiated in the presence of convection, it was fine (<0.5 cm. dia.).

A. Introduction

Ingot macrostructures are generally classed as containing one or more of the three zones: "chill zone", "columnar zone", and central "equiaxed zone". These three zones are sketched in Figure 1; their origin has been discussed in some detail[1-7].

The classical explanation for formation of the chill zone is that supercooling occurs in the region of liquid metal adjacent the mold wall, and copious nucleation then takes place in this region forming numerous small crystals. The columnar region results by growth of favorably oriented grains (dendrites) which crowd out their less favorably oriented neighbors[1,4].

The mechanism of the columnar-equiaxed transition has been the subject of considerable interest. The generally accepted mechanism, until recently, was that constitutional supercooling developed in front of the growing columnar grains with eventual nucleation of new, equiaxed, grains ahead of the growing solid front[2]. Recently, it became evident this explanation was not completely satisfactory and it is now evident that "crystal multiplication" plays an important role. This crystal multiplication occurs by separation of dendrite arms from growing dendrites[6,8,9], and has been shown to be strongly influenced by convection[6,10-13]. Reduced convection results, for a given alloy, in longer columnar zone, larger columnar grains, and larger equiaxed grains[7,12].

In this work, it is shown that convection has a similar strong influence on formation of the "chill zone". The work was conducted on small laboratory test specimens, but results are expected to be applicable to solidification of much larger castings and ingots. Certainly in large castings and ingots, substantial convection is present during initial solidification, when the "chill zone" forms. This convection arises from pouring momentum as well as from temperature differences in the molten metal.

B. Grain Structures Obtained

Apparatus employed to obtain rapid solidification against a chill wall while minimizing convection is sketched in Figure 2. Liquid metal was drawn by partial vacuum into the thin section mold cavity. The mold was copper; internal mold surfaces were polished and coated with amorphous carbon prior to casting. Plates cast were 5 cm. wide and usually 7.5 cm. high; thicknesses cast were 0.1 cm., 0.32 cm., and 0.95 cm. Alloy was aluminum-4.5 per cent copper.

As will be shown below, (1) the casting apparatus described above permitted completely filling the mold cavity before any solidification took place, (2) solidification, when it then began, took place in relatively quiescent liquid, but (3) very rapid solidification rates were obtained, at least as rapid as at the metal surface of usual ingots. Using an alternate procedure, solidification could be initiated before filling was complete, thereby causing freezing to take place in a rapidly moving stream.

Structure of two typical castings are shown in Figure 3. The structures shown are the surfaces of the plate castings as they appear after removal from the mold. Dendrites are delineated by surface shrinkage, without polishing or etching. The structures are of plates cast at 140 and 220°C above the liquidus temperature of the alloy. They are typical of those obtained in all plates cast at sufficiently high superheats. Note the grain size in these plates is large, some grains covering an area in excess of one square centimeter.

Increasing superheat temperature (above a critical temperature discussed below) has no significant effect on surface grain size, and increasing plate thickness in the range of 0.1 to 0.95 cm. increases grain size only slightly.

For a given set of casting conditions, there is a minimum superheat temperature below which the surface grain size changes discontinuously. This critical superheat decreases with increasing plate thickness and with decreasing filling time. Figure 4 shows two typical castings (0.1 cm. thick) filled under the same pressure differential (4 cm. Hg) at different superheat temperatures. The grain size is seen to be large ($\tilde{>}$1 cm. dia.) in the casting poured at higher superheat and very fine (<0.5 cm. dia.) in the casting filled at lower superheat.

Filling time was measured in several castings made in identical fashion to the four above. This was done by placing exposed wires at the top and bottom of the mold cavity, and measuring the time (using an oscilloscope) required for the molten metal to travel between the two wires. Filling time was approximately 0.1 seconds.

The two castings in Figure 4 were filled at relatively rapid rate. In castings filled at slower rate, duplex structures are often obtained, particularly when filling is incomplete. Figure 5 shows two such structures. Grains at the upper portion of each casting are fine, while those at the lower portion are coarse. A general characteristic of castings with duplex structures is that the last metal to enter the mold cavity is the metal which solidifies with the coarser structure.

C. Interpretation of Structures

Rate of heat extraction from plate castings such as those made herein is limited exclusively by mold-metal interface resistance when the Nusselt number is small compared with one, i.e.,

$$\frac{hL}{k} << 1 \qquad (1)$$

where: h = mold-metal heat transfer resistance

L = half plate thickness

k = metal thermal conductivity

For aluminum cast in copper molds, coated with amorphous carbon, h has been shown experimentally to be about .04 cal./cm.^{2}sec.°C[14]. The thermal conductivity of liquid as well as solid aluminum is in excess of .1 cal./sec.cm.°C for aluminum so $\frac{hL}{k} << 1$ for even the heaviest plate ($2L = .95$ cm.) cast in this study. Hence, no significant temperature differences can be expected across the plate thickness before, during, or after solidification, and cooling rate of the liquid in the mold cavity prior to solidification is given simply by Newton's Law of Cooling:

$$\frac{dT}{dt} = \frac{h(T - T_o)}{L\,\rho'\,C'} \qquad (2)$$

where: $\frac{dT}{dt}$ = rate of temperature change of the liquid in the mold cavity prior to solidification.

T = liquid temperature

T_o = mold temperature

ρ' = density of liquid aluminum

C' = specific heat of liquid aluminum

Substituting reasonable numerical values in equation (2) ($T - T_o = 700$°C, $\rho' = 2.7$, $C' = .26$), $\frac{dT}{dt}$ is approximately 800°C/sec. for the 0.1 cm. thick plate. For the filling conditions of the castings in Figure 4 (measured filling time, 0.1 sec.), total temperature drop during filling is calculated from equation (2) as approximately 80°C. Hence, for the castings poured at superheat temperatures greater than about 80°C, the mold was full before any solidification occurred in the mold cavity.

On the other hand, in the plates cast at less than about 80°C superheat, solidification must have been initiated prior to cessation of flow. This is clearly true, for example, in the plate cast at approximately 20°C superheat, Figure 4a, which began to solidify before filling was complete (preventing complete filling). In these plates, initial solidification took place in a rapidly flowing stream. Flow velocity when the plates are half filled is about 100 cm./sec.)

After bulk flow ceases, when the mold is full, one expects localized eddy currents. However, in the thin plates these are expected to quickly dissipate and, at least for the higher pouring temperatures, such currents must be low when solidification is initiated. The currents are expected to die out in a time τ the order of L^2/ν,[15] where ν is the kinematic viscosity. For the 0.1 cm. plate, $L = 0.5$ and $\nu = .01$, so $\tau \approx 0.25$ seconds. Hence, again using the 0.1 cm. thick plate as example (0.1 sec. filling time), a superheat temperature of 280°C is calculated (from equation 2) as necessary to allow both complete filling and essentially complete decay of residual eddy currents before solidification begins. This amount of superheat has not, however, been found necessary. Plates 0.1 cm. thick have been cast with coarse grains at superheat temperatures as low as 200°C.

It is of interest that, since the metal at the tip of the stream enters the mold cavity first, a substantial temperature gradient exists in the metal during the filling period in a direction parallel to the casting length. The tip of the stream is coldest. The duplex structures in Figure 5 result because of this temperature gradient. Solidification at the tip of the stream was initiated during flow, and hence a fine-grained structure results. The superheated metal at the lower part of the castings began to solidify only after flow ceased and the structure in the region is therefore coarse-grained.

Also, it is noteworthy that the very coarse grains obtained in this work were formed at extremely rapid cooling rates compared with those present in ingot solidification, even in solidification of the chill zone. Cooling rate was calculated (from equation 2) as 800°C/second for the 0.1 cm plate above, and a solidification time, t_f, can be calculated by writing Newton's Law for removing heat of fusion:

$$t_f \cong \frac{LH\rho}{2h(T_L - T_o)} \qquad (3)$$

where: H = latent heat of fusion

T_L = liquidus temperature of alloy

Several experiments were conducted to determine that the value of .04 cal/cm^{2}sec°C used for h was approximately correct. Cooling curves were made in both .1 cm and .95 cm thick castings. The thermocouple used was unprotected thirty gauge iron-constantan wire. Results were recorded photographically on an oscilloscope for the 0.1 cm thick casting and on a high speed recorder for the 0.95 cm thick casting. Change of slope in the cooling curve indicates precisely onset of freezing, and the long freezing range of the alloy[16] allows an accurate determination of total solidification time.

For plates 0.1 cm thick, measured freezing times were 0.5 to 0.8 seconds. For the .95 cm thick casting, measured freezing time was 7.6 seconds. These results are in close agreement with calculation using equation (3), if h is taken as 0.04. (Calculated values of t_f are 0.7 sec. and 7 sec. for the 0.1 cm. plate and 0.95 cm. plate, respectively.)

D. Conclusions

Large surface grains (>1 cm. dia.) can be obtained in rapidly solidified laboratory ingots provided solidification takes place in a convection-free melt. The fine-grained equiaxed "chill zone" is obtained only in the presence of convection. It is therefore concluded that earlier explanations of chill zone formation, based on copious nucleation from local undercooling, must be modified.

REFERENCES

1. F. R. Henzel, Trans. A.I.M.E., 124, 300 (1937).

2. W. C. Winegard and B. Chalmers, Trans. Am. Soc. Met., 46, 1214 (1954).

3. J. L. Walker, "Liquid Metals and Solidification", pp. 319-336, A.S.M., Cleveland, Ohio (1958).

4. B. Chalmers, J. Australian Inst. Met., 8, 255 (1963).

5. B. Chalmers, Principles of Solidification, pp. 253-297, John Wiley, New York (1964).

6. K. A. Jackson, J. D. Hunt, D. R. Uhlmann, and T. P. Seward III, Trans. Met. Soc. A.I.M.E., 236, 149 (1966).

7. D. R. Uhlmann, T. P. Seward III, K. A. Jackson, and B. Chalmers, to be published.

8. A. Papapetrou, Z. Krist., A92, 89 (1935).

9. M. O. Klia, Kristallografia, 1, 577 (1956).

10. F. A. Crosley, R. D. Fisher and A. G. Metcalfe, Trans. Met. Soc. A.I.M.E., 221, 419 (1961).

11. F. C. Langenberg, G. Pestel, and C. R. Honeycutt, Trans. Met. Soc. A.I.M.E., 221, 993 (1961).

12. M. C. Flemings, H. F. Utech and E. S. Miksch, "Effect of Fluid Flow on Solidification Structure", Technical Report No. 1 to the Office of Naval Research, Contract NONR-3963(09), March 1966.

13. G. S. Cole and G. F. Bolling, Trans. Met. Soc. A.I.M.E., 233, 1568 (1965).

14. T. F. Bower, H. D. Brody and M. C. Flemings, Annual Report, Contract No. DA-19-020-ORD-5706(A), June 1963 - June 1964, for Department of Army, Material Command, MUCOM, Frankford Arsenal, Philadelphia, Pennsylvania, 19137.

15. R. B. Bird, W. E. Stewart, and E. N. Lightfoot, Transport Phenomena, John Wiley, New York (1960).

16. T. F. Bower, H. D. Brody and M. C. Flemings, Trans. Met. Soc. A.I.M.E., to be published, 1966.

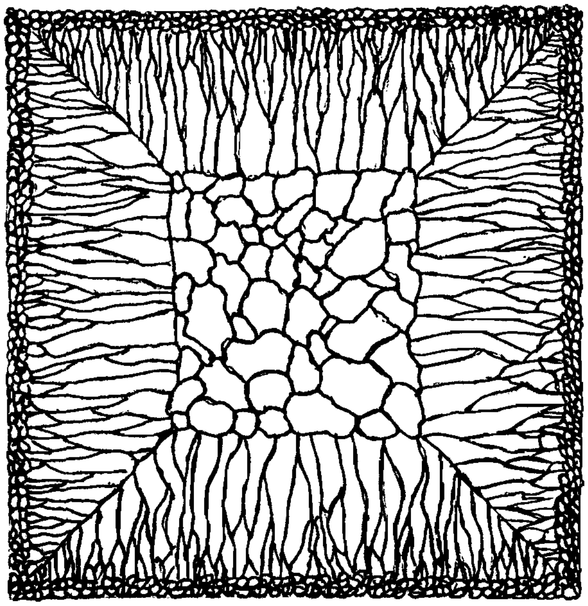

Figure 1: Sketch of a chill zone, columnar zone, and equiaxed zone.

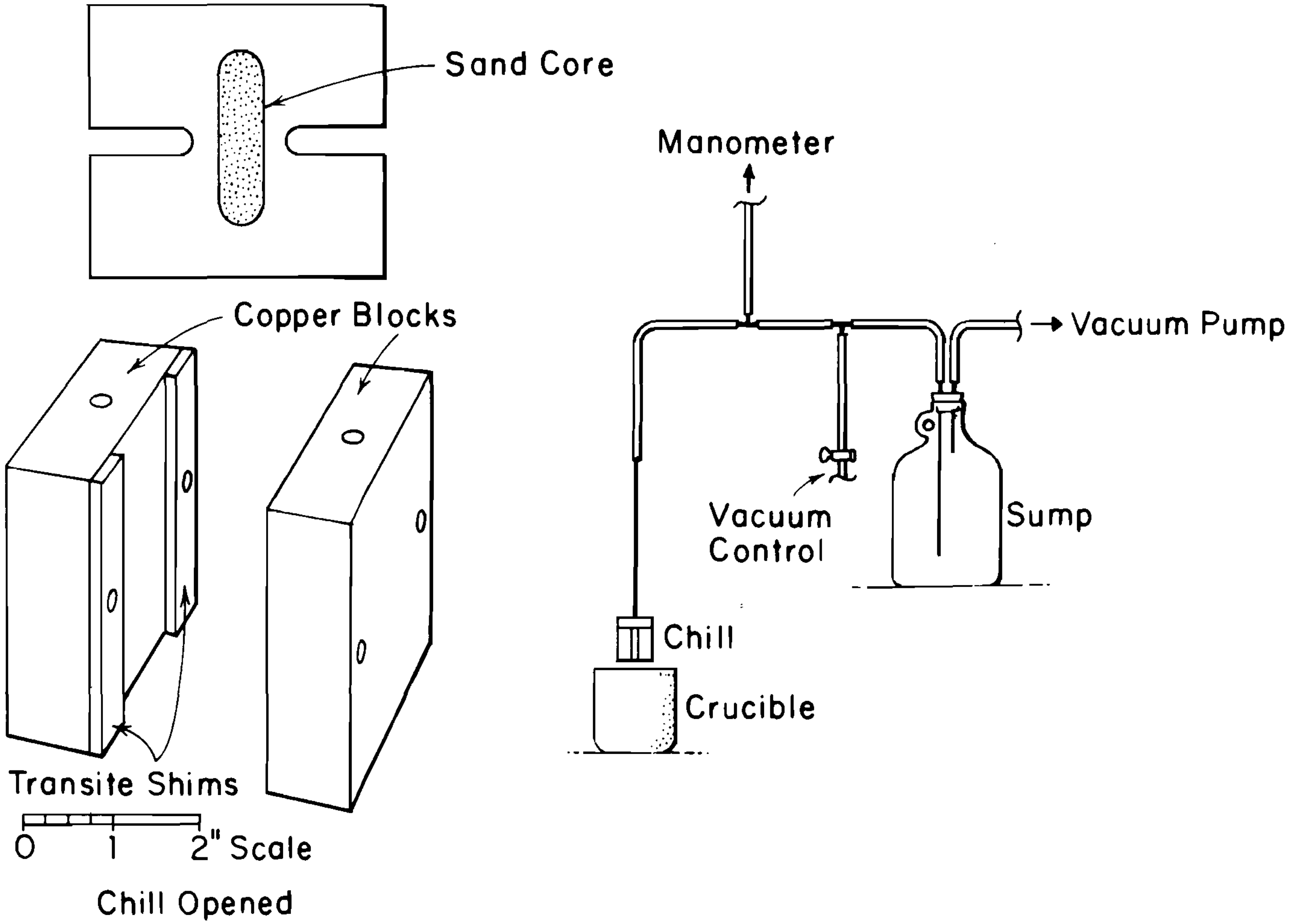

Figure 2: Apparatus to obtain rapid solidification against a chill wall while minimizing convection.

(a)

(b)

Figure 3: Coarse grained chill plates cast at 140 and 220°C above the liquidus temperature.

(a) .32 cm. thick, 870°C, 3 cm. Hg
(b) .95 cm. thick, 790°C, 3 cm. Hg

[Grain boundaries are outlined by pen in (a).]

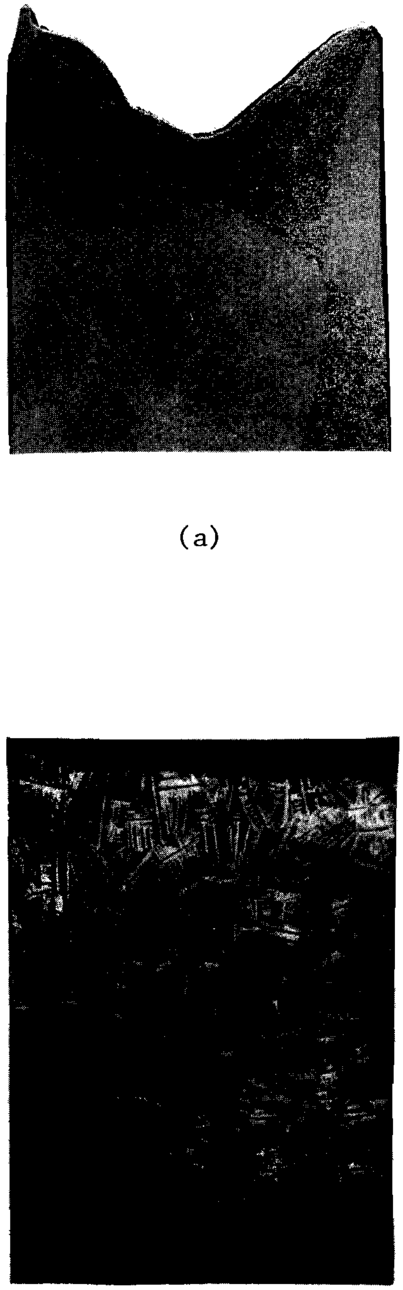

(a)

(b)

Figure 4: Two typical castings filled under the same pressure differential (4 cm. Hg) at two different superheat temperatures. Both are 0.1 cm. thick, and 5 cm. wide. (a) 670°C (b) 850°C.

(a)

(b)

Figure 5: Duplex grain size found in partially filled mold.

(a) Typical of 1 mm. thick castings, "poured" at 700°C

(b) A .32 cm. thick mold which failed to fill completely.

Chapter 4: STRUCTURE OF DENDRITES AT CHILL SURFACES

ABSTRACT

Results are reported of a study of surface dendritic structure of an aluminum-copper alloy solidified against a chill wall. The structure is readily apparent, without polishing or etching. Most primary and secondary "arms" in the surface dendritic structure are arranged orthogonally, giving the impression of strong preferred orientation on the surface. However, no such preferred orientation exists and it is therefore evident the "arms" do not represent <100> directions.

The primary "arms" are shown to be intersections of a {100} plane with the chill plane or, more rarely, the projection of a <100> direction on the chill plane. Traces of secondary dendrite "arms" are usually within a few degrees of 90° to the primary trace independent of dendrite orientation. Primary, secondary and higher order dendrite traces almost always represent intersections of {100} planes with the chill surface, or projections of <100> directions.

Dendrite traces are often observed to be bent. In these cases the crystal lattice changes orientation; bending is concave to the chill surface.

A. Introduction

In a previous chapter, a technique was discussed whereby large grains can be obtained under very high cooling rates at a chill surface. The technique used involves quickly drawing liquid aluminum into a thin copper mold; when sufficient superheat exists in the liquid, grains grow without convection in the liquid and the grain size is large. The chill surfaces employed are polished copper blocks coated with amorphous carbon. Shrinkage during solidification between dendrite arms and grains delineates both, without the need for polishing or etching of the cast surface. Thus the as-cast chill surface is readily observed.

In the previous chapter, the grain structure of the chill surface grains was discussed, primarily the effect of convection on grain size. In this chapter, the dendrite arms within each grain are examined.

The literature on chill surface dendrite studies is rather limited. Edmunds studied the development of preferred orientation in zinc, cadmium, and magnesium[1]. In zinc and cadmium he found that the surface region has a (0001) texture (parallel to the chill surface). Walton and Chalmers reasoned that the fast growth <10$\bar{1}$0> directions are in the basal plane so that a ". . . small crystal in a supercooled melt will grow as a flat plate parallel to the basal plane . . . The nuclei that grow parallel to the mold wall would produce larger grains than nuclei with other orientations. These larger grains would have a basal plane parallel to the mold wall and a preferred orientation could be observed to exist on the ingot surface".[2]

The same authors, in measurements on aluminum ingots, found no preferred orientation at the mold wall. However, the X-ray technique they used measured the preferred orientation in terms of grain numbers, not grain areas; larger grains were weighed equally with small ones. No preferred orientation is expected on this basis at the chill surface. In a later paper[3], Edmunds stated that experiments show a random grain orientation texture at the surface in die cast aluminum; his technique, also used in his earlier paper, takes account of grain area.

No work seems to have been published on the dendritic structure of chill grains. Biloni and Chalmers have recently published a paper on "predendritic growth", showing the change in morphology from spherical to dendritic during the initial stages of freezing[4]. They did not study the clearly defined dendrite patterns obtained on the graphite chill used in their study.

Lindenmeyer has investigated the growth of ice dendrites under varying conditions[5]. When growth was on a substrate, the dendrite axes were bent. The bend corresponded to a change in orientation of the crystal lattice and occurred in such a way as to align the basal plane to the substrate.

B. Dendrite Trace Geometry

Figure 1 shows the chill surface of a typical casting poured above the critical temperature necessary to produce coarse grains. A cursory examination of most grains shows that dendrite traces within most grains are oriented roughly perpendicular to each other. One is tempted to assume that the dendrite traces are <100> directions and that, therefore, marked preferred orientation exists at the chill face. This, however, is not the case.

Each of the grains in the casting of Figure 1 was separately identified (Figure 2) and its orientation determined by the Laue back reflection method. Results are given in Figure 3 and it is seen there that no preferred orientation exists. Even when grain area is accounted for, there is no significant preferred orientation.

Three typical grains are shown in Figures 4 - 6. In Figure 4 a grain is shown which lies on the <100> zone. Examination of the stereographic triangle shows that both of the traces (which are orthogonal) coincide with intersections of {100} planes with the chill surface. One set of traces is nearly a <100> direction but the second is not. The second trace aligns with the projection of a <100> direction which lies 25° out of the chill surface.

Figure 5 shows a dendrite of somewhat different orientation (grain No. 17 in Figure 2). Here again orthogonal dendrite traces are apparent, but only one set coincides with the intersection of {100} planes; the other set is aligned with the projection of a <100> direction on the chill face. In addition to the orthogonal dendrite traces in Figure 5, a third set (of non-orthogonal traces) is visible. These are aligned with intersections of a second set of {100} planes with the chill surface.

A third grain is shown in Figure 6. Here orientation is such that <111> is very nearly perpendicular the chill face (grain 60, Figure 2). Close inspection of the photograph and comparison with the stereographic projection for the grain shows that five different trace directions are present; three of these are intersections of mutually orthogonal {100} planes; two are projections of <100> directions.

Grains near the <111> pole always exhibited non-orthogonal dendrite traces; i.e., traces were intersections of more than one {100} plane, as well as projections of <100> directions. Dendrites whose orientation was such that they lay in the region marked "not orthogonal" in Figure 3 exhibited this characteristic. Dendrites whose orientation was closer to a <100> zone (in the region marked "orthogonal" of Figure 3) never exhibited non-orthogonal traces. In these grains traces were always the intersection of one set of {100} planes and one set of <100> directions. (For grains on or very near the <100> zone, such as Grain 65 of Figure 4, the projections of <100> directions are undistinguishable from intersections of {100} planes.) Grains in the "transition region" of Figure 3 sometimes showed non-orthogonal traces and sometimes did not.

Structure of surface dendrites, as in Figure 1, is often unsymmetrical with respect to the primary arms. Secondary dendrite traces on opposite sides of the primary trace can differ in two ways. First, the dendrite arms are often clearly defined on one side, and blurry on the other side. Second, the poorly defined arms are generally much shorter than those that are well defined (on the opposite side of the primary).

When the primary trace is the intersection of a {100} plane, the orthogonal secondaries are projections of <100> directions. In this case, only those <100> arms which are growing toward the chill develop clearly. Even for a 2° deviation from the chill surface, as in Figure 4(grain 65) the arms growing toward the chill are clearer than those growing away. Figure 7 shows a larger portion of grain 65 than is given in Figure 4; in this figure it can be seen further than tertiary arms associated with the 25° <100> direction develop only in one direction, toward the chill.

Figure 5 shows the effect clearly of preferential growth along the chill surface of arms whose <100> direction points into the surface. In this grain (grain 17), secondary arms at 90° occur only where a <100> direction points toward the chill. Again in Figure 6, the one well-developed set of <100> projections grow toward the chill from a non-orthogonal primary arm, but not away from it. In fact, well-developed <100> traces have not been found to result from growth away from the chill surface. Some surface grains do show symmetrical growth about a primary axis, as Grain 64 in Figure 2, but this apparently occurs only in grains having a <100> direction oriented very nearly parallel the chill surface, or in grains having secondary arms which are intersections of {100} planes.

It may be inferred from the foregoing that growth of surface grains along the chill surface proceeds as described below. It is assumed here that growth is initiated from a nucleus, or other growth center (such as a separated dendrite arm) that is a short distance from the chill into the melt; however, essentially similar growth is to be expected if nucleation is on the chill surface.

Growth is expected to proceed dendritically, with orthogonal branching, from the growth center into the undercooled metal adjacent the chill face. In the usual case, two sets of dendrite arms growing orthogonally in <100> directions within a (100) plane are expected to reach the chill simultaneously, and extension of this intersection of the (100) plane across the chill face then occurs rapidly, the trace of the plane becoming the primary dendrite "arm" on the casting surface.

Dendrite arms then presumably grow into the bulk melt in the third orthogonal <100> direction perpendicular to the (100) plane considered above. Those arms that are oriented so they strike the surface grow rapidly along the surface in the direction of the projection of the <100> direction; these then become the orthogonal secondary arms. Orthogonal tertiary arms form similarly and non-orthogonal secondary or tertiary arms form when well developed {100} planes reach the surface and extend as does the primary arm considered above.

In the rarer case where the primary dendrite arm is a projection of a <100> direction, this arm apparently grows as the secondary arm discussed above, and lower order arms grow as projections of directions or intersections of planes as described above.

C. Bent Dendrites

Bent dendrite traces can be seen on the chill surface of most of the castings made; particularly severe bending is shown in Figure 8. The radius of curvature of the primary traces varies from very large radii down to 1 or 2 centimeters in coarse grain structures as shown in Figures 1 and 8. Qualitative comparison of castings made indicates that more bending occurs the thinner the section thickness, and that dendrite bending is not dependent on pouring temperature.

Typically, the dendrites have Laue patterns similar to unbent dendrites, with sharp spots. Laue patterns were taken of these dendrites using an X-ray beam .02 inches diameter, small compared with the grain size. Orientation changes over distances the size of the X-ray beam are small. Over larger distances, however, the orientation changes may be very large indeed; a 40° change in orientation is not unusual.

There are two components of the orientation change which may be resolved. One component is the bend which is observable on the chill surface and can be described as a rotation of the crystal lattice about an axis perpendicular to the chill plane. The second component is a change in orientation in the stereographic projection; this component is rotation of the crystal lattice around an axis laying in the chill plane. All bent dendrites show a change in orientation in the stereographic projection. The dendrite trace which is bent may be either the projection of a <100> direction of the intersection of a {100} plane.

Consider the change in orientation in the stereographic projections along a bent dendrite. Figure 9a shows how the stereographic projection must move if the dendrite crystal lattice is concave toward the chill surface and Figure 9b illustrates that this is the case for the dendrite shown. All dendrites examined were found, like this one, to be concave to the chilled surface. It is not clear from our work whether this bending is due to thermal stresses on the growing dendrite, mechanical stresses, or to some other feature connected with growth of the dendrite in its early stages.

Figure 10 shows dendrites found in convection-refined grains[6]. Here radii of curvature as small as 1 millimeter can be seen. Laue photographs of this structure, as expected, do not give sharp spots, but rather clusters of spots and spots showing asterism. No study was made of the orientation changes in these grains. If fine grains are produced with a grain refiner but with no convection, no bending is apparent.

D. Summary

A new technique has been used for studying the surface structure of alloys cast against a chill. The technique involves solidification of a thin section casting in a smoothly polished metal mold.

The dendrite "arms" visible on the chill surface usually are orthogonal within a single dendrite. One set of orthogonal dendrite traces ("arms") consists of the projections of <100> directions onto the chill surface; the orthogonal set of "arms" consist of intersections of {100} planes with the chill surface. The orthogonal planes and directions have the same indices. Only those dendrite arms develop traces which grow toward the chill surface.

When a <111> direction in the dendrite lies nearly perpendicular to the chill surface, the dendrite arms do not appear orthogonal. In this case, two or three {100} plane intersect the chill surface and form dendrite traces. (The projection of one, two or three <100> directions may also be present.)

X-ray analysis of a large number of chill grains shows that their orientation is random. Also, the average grain size does not vary significantly for different orientations.

Dendrite bending occurs under some casting conditions. Moderate bending of dendrite traces can be seen in some large surface grains. This bending is concave toward the chill surface. The orientation change in these dendrites may be large from one end of the grain to the other. Bending in fine grains is much more severe, if these are produced in castings which solidify while the mold is filling under strong convection. The radius of curvature of bend in fine grains is one or more times smaller than the radius observed in coarse grains (at the chill surface).

REFERENCES

1. G. Edmunds, A.I.M.E. Trans., 143, 183 (1941).

2. D. Walton and B. Chalmers, Trans. Met. Soc. A.I.M.E., 215, 447 (1959).

3. G. Edmunds, A.I.M.E. Trans., 114 (1945).

4. H. Biloni and B. Chalmers, Trans. Met. Soc. A.I.M.E., 233, 373 (1965).

5. C. S. Lindenmeyer, Thesis, "The Solidification of Supercooled Aqueous Solution", Harvard (1959).

6. See Chapter 3 of this report.

Figure 1: Casting drawn at 730°C; 5 cm. wide by 0.95 cm. thick. The grains of this casting are outlined in Figure 2. The orientation of all numbered grains was determined by the Laue back reflection X-ray technique.

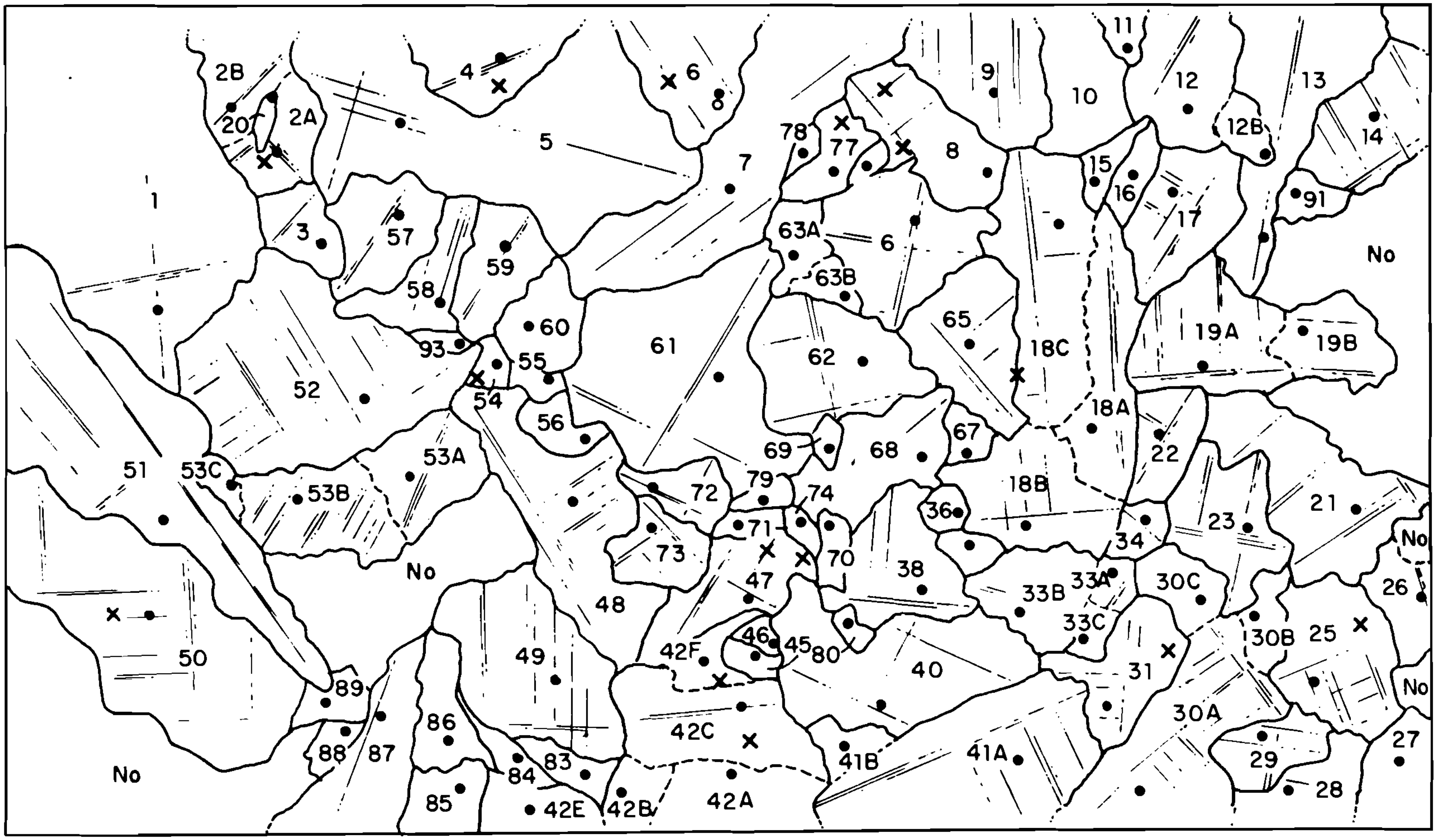

Figure 2: Grains of Figure 1, showing the numbering system used and the Laue X-ray spot location. Dots indicate orientations given in Figure 3. Crosses indicate other orientation determinations.

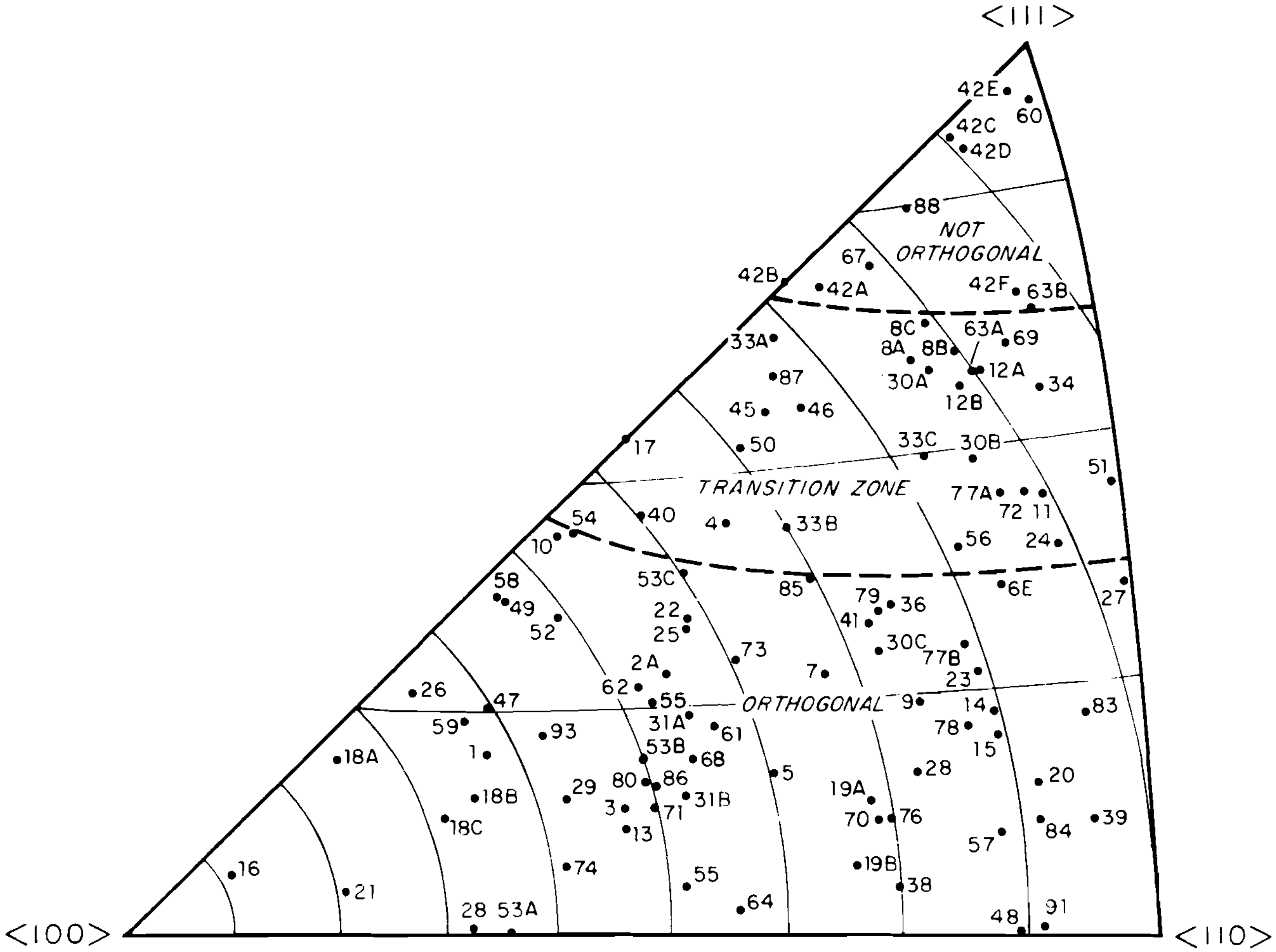

Figure 3: The orientation of grains of the casting shown in Figure 1. The variation of dendrite trace geometry from orthogonal to non-orthogonal is indicated.

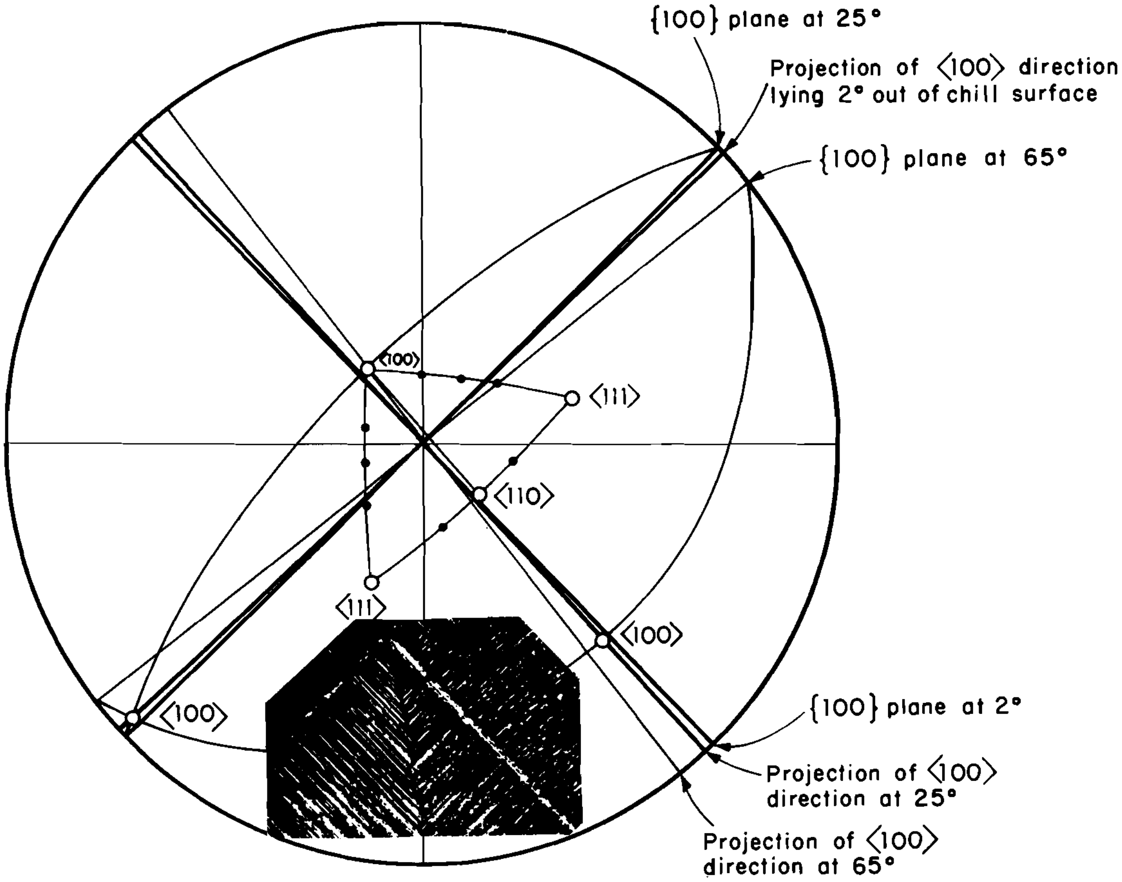

Figure 4: Stereographic projection of the Laue photograph of Grain 65 with the microstructure in a corresponding orientation. The dendrite traces of this grain, which lies on the <100> zone, are at 90°.

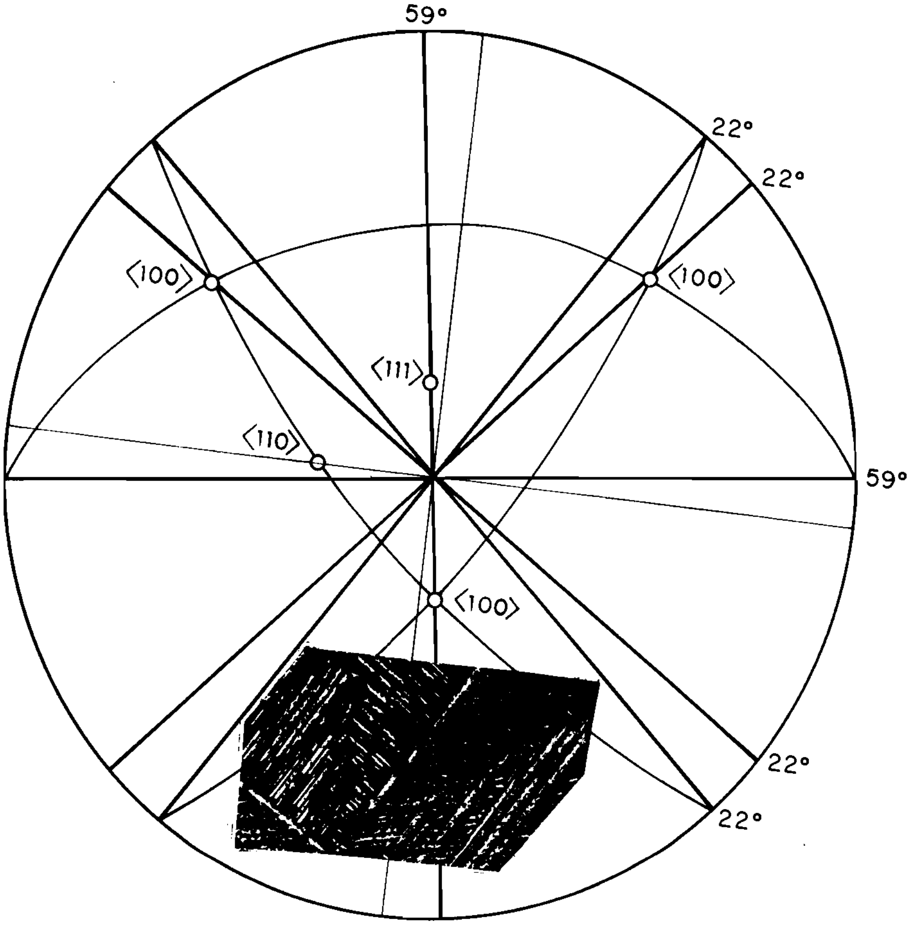

Figure 5: Stereographic projection and corresponding photomicrograph of Grain 17. This grain is oriented between <111> and <100>, as shown. Of the orthogonal dendrite traces, one set corresponds to intersections of {100} planes with the chill surface, the other set to projections onto the chill surface of <100> directions of like indices. A second set of {100} planes (intersecting the chill 59° from perpendicular) makes nonorthogonal traces on the chill surface.

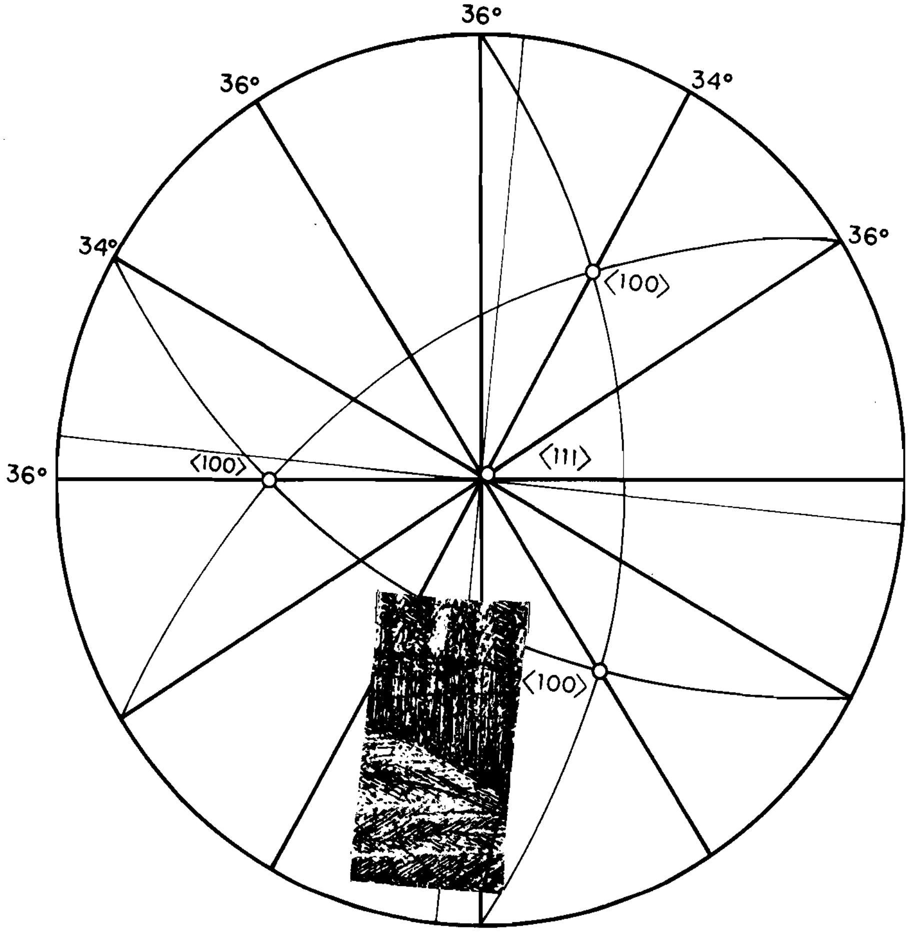

Figure 6: Stereographic projection and corresponding photomicrograph of Grain 60. A <111> direction of this grain is almost perpendicular to the chill surface. Traces representing the intersection of all three {100} planes can be seen in the photomicrograph. Also, one projection of a <100> direction is strongly developed (sloping from left to right, almost horizontal in the picture).

(a)

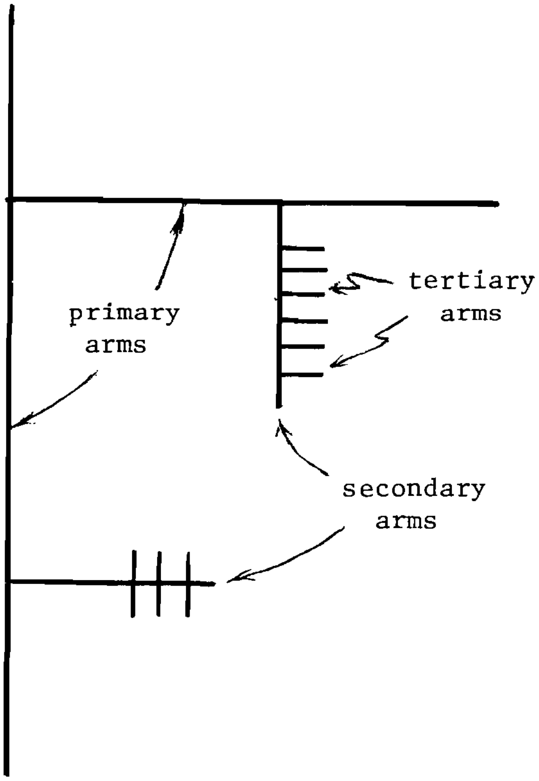

(b)

Figure 7: (a) Grain 65 of Figures 2 and 4 (50X).
(b) Terminology used in discussion of surface dendrite arms.

Figure 8: Casting drawn at 760°C; 5 cm. wide by 0.32 cm. thick. One micron alumina spray coating used instead of amorphous carbon coating.

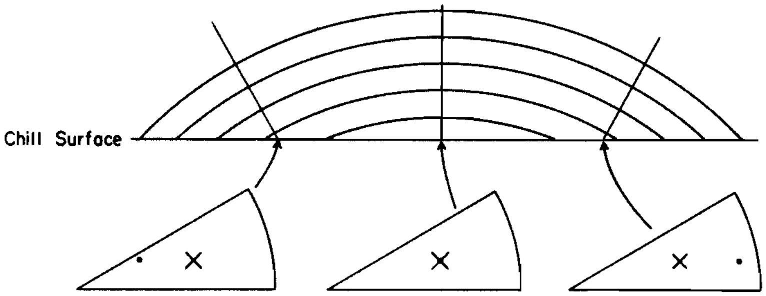

a. Schematic Concave to Chill. Orientation at Arrowhead is Represented by the Dot in the Stereographic Triangle.

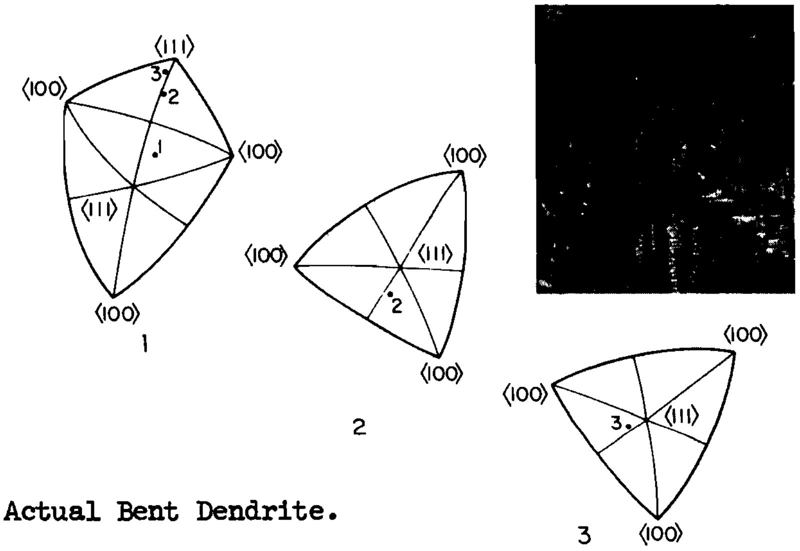

b. Actual Bent Dendrite.

Figure 9: Analysis of bent dendrite. a. Schematic diagram of crystal lattice with a bend concave to the chill surface and corresponding orientations at various points, indicated in stereographic triangles. Looking from left to right, the orientation dot moves from left to right in stereographic triangle. b. Bent dendrite from Figure 8 (3X) and portions of the stereographic projections at points 1, 2 and 3 on the bent dendrite trace. The bend of the dendrite corresponds to a; it is concave to the chill surface. The bending observable in the chill surface is reflected in a corresponding rotation of the stereographic projection from 1 to 2 to 3.

Figure 10: Convection - refined grains (50X).

Chapter 5: NON-DENDRITIC SOLIDIFICATION

ABSTRACT

Experiments were conducted on dendritic and non-dendritic solidification of aluminum-copper alloys and of a magnesium-zinc alloy. Grain diameter in the non-dendritic melts was found to depend on solidification time in quantitatively the same way as dendrite arm spacing in the dendritic melts.

An explanation of the above results is given based on structure coarsening ("ripening") during solidification. It is concluded that "dendrite element spacing" (arm spacing in the dendritic melts, grain diameter in the non-dendritic melts) is determined not by how many elements form during initial growth, but rather by how many such elements disappear by ripening during growth. Quantitative agreement is obtained between experimental results and a theoretical equation based on coarsening kinetics.

Microsegregation (as measured by amount of second phase) is shown to be substantially less in the non-dendritic aluminum and magnesium base alloys than in the comparable dendritic alloys.

A. Introduction

In Chapter 4 of last year's annual report[1] consideration was given to methods of achieving a grain size in cast structures as small as, or smaller than, dendrite arms in the non-grain refined structure. Such a structure was expected to solidify non-dendritically. Further, if the grain size were sufficiently small it was expected to possess reduced microsegregation.

Experiments were described in the last annual report which showed that through use of a vibrating chill rod, combined with slow solidification, such a non-dendritic structure could be obtained in aluminum alloys. The work confirmed that microsegregation in an alloy so solidified was much reduced.

The above work was continued herein. A series of aluminum alloys was solidified using the same basic apparatus described earlier. Two typical structures are shown in Figures 1 and 2. Figure 1 shows the microstructure of aluminum-4.5 per cent copper alloy solidified in 12 hours and water quenched from just below the eutectic temperature. Mean grain size * is approximately 350 microns, only slightly less than would be the dendrite arm spacing at this solidification time. However, microsegregation is much reduced.

Figure 2 shows the structure of a 7075 alloy ingot solidified similarly except that it was water quenched when it was less than 25 per cent solid; time of cooling from the liquidus temperature to quench temperature was three hours. Grain size is approximately 50 microns. Grains are non-dendritic but in this, as in all other tests

---

* Grain size was determined by the lineal intercept method (see equation (2). "Grain diameter" as will be shown later, is somewhat larger.

performed, grain size obtained was not greatly smaller than the dendrite arm spacing in unrefined specimens (solidified at similar rate).

It was evident from the foregoing work that grain size and cooling rate are not completely independent variables in non-dendritic structures (as they can be in dendritic structures). In spite of the "grain multiplication" technique employed[1] (vibrating chill rod) final grain size achievable was found to be a strong function of solidification time, increasing with increasing solidification time, as does dendrite arm spacing. This rather surprising result led to work described below, aimed at obtaining a more detailed fundamental understanding of solidification and microsegregation in non-dendritic solidification.

B. Non-Dendritic Solidification in Magnesium Base Alloys

Commercial non-ferrous casting alloys in which solidification is non-dendritic include those of the magnesium-zinc system, grain refined with zirconium. Omission of the zirconium from the melt produces a coarse grained structure with usual dendritic appearance. Because of the relative ease with which the non-dendritic structure can be obtained, this system was selected for detailed study on effects of solidification variables on structure in non-dendritic solidification.

C. Melting and Casting

The bulk of work was conducted on four sand cast plates, of dimensions 9" x 6" x 3/4" thick. Two of these were of grain refined magnesium-5.5 per cent zinc alloy, and two of non-grain refined magnesium-5.5 per cent zinc alloy. The alloys were melted in a clean steel crucible using standard magnesium melting and alloying techniques.

One casting in each alloy was unchilled, and allowed to cool to room temperature in the sand mold; the other was end-chilled as described earlier[1], and allowed to cool to room temperature in the mold. Four thermocouples were inserted in each casting to measure solidification times. Thermocouples were 2 inches apart along the longitudinal centerline.

In addition to the four castings above, a fifth was made of metal that was not grain refined and not chilled. This casting was water quenched as it cooled to just below the eutectic temperature, in order to examine any possible effect of solid state diffusion after solidification on final segregation. Finally, to examine structure in metal solidified at very high rate (solidification times in the range of 0.5 to 10 seconds), several small samples of metal were cast against large chills. Table I summarizes the plate castings poured.

D. The Magnesium-Zinc Phase Diagram

The equilibrium diagram of the system magnesium-zinc has been investigated by a number of workers[2-7]. Despite a substantial body of literature on the subject there still exists considerable confusion as to its constitution over a wide composition range. Published work by Clark and Rhines[7], who redetermined the phase equilibria in the magnesium-zinc system from 0 to 85 weight per cent zinc, verified the existence of the Mg_7Zn_3 phase. The reported value of the composition Mg_7Zn_3 is 53 weight per cent zinc, which is just slightly higher than the eutectic composition. Mg_7Zn_3 is not stable at low temperatures but undergoes a eutectoid decomposition at a temperature not far below that of the eutectic. It can easily be retained at room temperature, since its transformation kinetics are sluggish[8,9].

In order to achieve better accuracy in quantitative analyses, the electron microprobe was used in the course of this work to analyze the second phase present. The results from these measurements confirmed that Mg_7Zn_3 is retained at room temperature and that its composition is close to 53 weight per cent zinc. The rest of the phase diagram used for analyses herein is based on a survey of the work of several investigators[3,4,7], and is shown in Figure 3.

Based on the above phase diagrams, and on other assumptions[10] including no diffusion in the solid, zinc composition across dendrite arms can readily be calculated. Results are plotted in Figure 4 for the 5.5 per cent zinc alloy; 7.0 weight per cent eutectic is expected in the final structure. The measured composition of the melt that was not grain refined was slightly lower (5.2 per cent) and for this composition 6.9 weight per cent eutectic is predicted. The grain refined alloy was slightly higher in zinc content (5.9 per cent) and for this composition, 8.0 weight per cent eutectic is predicted in the final structure.

E. Structures Obtained

Typical structures obtained in non-grain refined material are shown in Figures 5 through 8, and typical structures of grain refined samples are shown in Figures 9 and 10. Table II summarizes data on dendrite arm spacing, casting type and location, and measured solidification time[5]. Dendrite arm spacings and grain sizes are also listed in Table II and are plotted in Figure 11 as a function of solidification time. These measurements were made as described below.

1. Measurements of Dendrite Arm Spacing.

Magnesium base alloys belong to the hexagonal system and thus the secondary dendrite arms are inclined at an angle to each other. The perpendicular distance between adjacent secondary arms was taken as the characteristic dendrite element spacing, and the measurements were made on photomicrographs at a magnification of 55X. For each measurement the average spacing was taken of several grains. All work was done on equiaxed grains.

Data are summarized in Table II and Figure 11. The equation of the solid line drawn through the data in Figure 11 is:

$$d_f = 5.5 \times 10^{-4} \, t_f^{\,0.4} \qquad (1)$$

where: d_f = average dendrite element spacing (cm)

t_f = solidification time (seconds)

2. Measurements of Grain Size.

Grain size measurements on the non-dendritic equiaxed magnesium-zinc-zirconium alloy were made by running a number of random traverses across photomicrographs of the samples and counting the number of grains intercepted by the line. The alloy was considered to consist of contiguous α grains, which is a good assumption since the volume fraction of the α-phase is almost equal to one. The mean lineal intercept was then obtained from:

$$\bar{L} = \frac{1}{N_L} \qquad (2)$$

where: $\bar{L}$ = average lineal intercept in three dimensions ("grain size")

N_L = number of grains intersected per unit length of test line

The actual grain diameter must, intuitively be larger than the mean grain size measured above. A simple statistical analysis yields the following relation[11]:

$$\bar{D} = 1.5\,\bar{L} \qquad (3)$$

where: $\bar{D}$ = "grain diameter"

The grain diameters are presented in Table II and on the same plot as the dendrite arm spacing versus solidification time, Figure 11. Note that these data correspond to essentially the same relationship as that of dendrite arm spacing versus solidification time.

F. Interpretation of Structures

The foregoing illustrates clearly the surprising result that grain size in grain refined magnesium-zinc alloy, and dendrite arm spacing in the un-grain refined alloy depend on solidification conditions in precisely the same way. This is in spite of the fact that grain size is usually thought to depend on rate of nucleation, while dendrite arm spacing is expected to depend on growth conditions.

The apparent anomaly is resolved only in the light of analyses of structure coarsening ("Ostwald ripening") during solidification[12-16]. From a recent study on undercooled metallic alloys (analytical and experimental) it has been shown that solidification structures are determined in large measure by this coarsening. For example, in dendrites, it appears that the final dendrite arm spacing observed is not strongly dependent (if at all dependent) on the dendrite arm spacing which initially forms. Instead, the final arm spacing is apparently determined primarily by how many arms disappear during the solidification process (by dissolution and reprecipitation on other, larger, arms[16].)

Similar results are obtained in non-dendritic structures from the highly undercooled alloy melts. Here, the number of growing grains decreases by many orders of magnitude during solidification, and conclusive evidence has been obtained to show the final grain size is determined only by coarsening kinetics; the initial number of nuclei formed being of only negligible importance. An approximate equation describing final dendrite element spacing*, derived by Kattamis and Flemings[16] and discussed in more detail in the next chapter is:

$$d = A\,(\bar{M}t_f)^n \tag{4}$$

where:

$$\bar{M} = \frac{2\sigma D_L T_L \ln \dfrac{C_E}{C_o}}{H(1 - k)m_L(C_E - C_o)} \tag{4a}$$

d = average final dendrite element spacing*, cm

t_f = solidification time, sec

σ = liquid-solid surface energy, cal/cm^2

D_L = liquid diffusion coefficient, cm^2/sec

T_L = equilibrium liquidus temperature, °K

H = volumetric heat of fusion, cal/cm^3

C_E = eutectic composition, weight per cent

---

* "Dendrite element spacing" is defined as dendrite arm spacing in dendritically solidifying melts and grain diameter in non-dendritic structures.

C_o = initial liquid composition, weight per cent

k = equilibrium partition ratio, dimensionless

m_L = liquidus slope (°K/%)

A,n = constants

The foregoing expression relates dendrite element spacing directly to alloy variables, and to solidification time, and is therefore expected to find considerable engineering usefulness. The engineering importance of the expression is that for the first time:

(1) It appears the mechanism controlling final dendrite arm spacing in castings and ingots has been established,

(2) It should be possible to correlate experimental measurements on dendrite arm spacings from different alloys and different alloy systems, and

(3) It should be possible to predict at least semi-quantitatively the influence of alloy variations or other process variables on dendrite arm spacing.

The data of Figure 11 have been replotted in Figure 12 as d versus $\bar{M}t_f$. $\bar{M}$ has been calculated using numerical values for the metal constants given in Table III. By comparison with Figures 8 and 9 of Chapter 6 it will be seen that essentially identical relations are obtained for d versus $\bar{M}t_f$. The three curves are the same within the uncertainties of the data employed. Hence, dendrite arm spacings are shown to depend only on $\bar{M}t_f$, for magnesium-zinc and for a variety of aluminum-copper alloys, solidified under a wide range of casting conditions.

G. Microsegregation

Microsegregation in the dendritic and non-dendritic magnesium-zinc structures was measured by lineal analysis of amount of second phase. For this purpose a Hurlbut Counter was used[17]. The apparatus and its application to quantitative metallography have been described in detail by Howard and Cohen[18]. Measurements of the volume fraction Mg_7Zn_3 were converted to weight fractions using a value of the density of Mg_7Zn_3 of 2.95 g/cc. Results are reported in Table II and Figure 13.

Measured values of weight per cent eutectic in the dendritic specimens are plotted in Figure 13, top, versus solidification time. The amount of second phase decreases with increasing solidification time due, presumably, to increased diffusion in the solid during solidification at the longer solidification times. Data from the quenched specimens show slightly higher amounts of eutectic than the unquenched specimens, indicating some homogenization occurred in the unquenched specimens during cooling to room temperature. However, the amount of this homogenization was small.

It has been shown that the extent of diffusion in the solid during freezing should be a single valued fraction not of solidification time, but of solidification time divided by the square of the dendrite arm spacing (e.g., η where $\eta = t_f/(d/2)^2$). In Figure 13, bottom, weight per cent eutectic is plotted against η and is seen to vary in a quantitatively similar way as predicted by detailed calculations for an aluminum alloy[10].

The maximum amount of eutectic found experimentally (at low values of η) is 6.6 weight per cent. This is approximately the amount calculated by the Scheil equation, Figure 4 (assuming no diffusion in the solid).

Figure 13 also shows the results for the non-dendritic specimens. At a given solidification time, t_f (or a given value of η), amount of second phase is substantially less in the grain refined (non-dendritic) castings than in the coarse grained castings. This is in spite of the fact that grain diameter in the fine grained samples varies as does the grain size; it is also in spite of the fact that alloy content was somewhat higher in the fine grained specimens (5.9 per cent) than in the coarse grained specimens (5.2 per cent).

The explanation for the lower eutectic clearly must lie in the different geometries of the two systems. Apparently the spherical geometry (perhaps because of its higher surface to volume ratio) permits greater diffusion in the solid during solidification.

H. Conclusions

1. Results illustrate that in non-dendritic solidification of non-ferrous metal alloys, final grain size is determined primarily by coarsening kinetics, as is dendrite arm spacing in coarse grained melts. It therefore appears unlikely that grain sizes can be achieved in castings or ingots which, at a given cooling rate, are substantially below the dendrite arm spacing achieved in coarse grained melts.

2. However, the fine non-dendritic grains which can be produced (e.g., in aluminum-4.5 per cent copper and magnesium-5. 5 per cent zinc) possess substantially reduced microsegregation in comparison with their dendritic counterparts. The reduction of severity of microsegregation is significant. For example, in magnesium-5.5 per cent zinc, up to 6.6 per cent eutectic by weight was found in the coarse grained cast structure. Less than 2 - 3 per cent was observed in the non-dendritic structures.

REFERENCES

1. T. F. Bower, H. D. Brody and M. C. Flemings, Annual Report, Contract No. DA-19-020-ORD-5706(A), June 1963 - June 1964, for Department of Army, Material Command, MUCOM, Frankford Arsenal, Philadelphia, Pennsylvania, 19137.

2. G. Grube, "The System Magnesium-Zinc", Z. für Anorganische Chemie, 49 (1906), p. 77.

3. R. Chadwick, "The Constitution of the Alloys of Magnesium and Zinc", J. Inst. Metals, 39 (1928), pp. 285-300.

4. W. Hume-Rothery, and E. O. Rounsefell, "The System Magnesium-Zinc", J. Inst. Metals, 41 (1929), pp. 119-136.

5. T. Takei, "The Equilibrium Diagram of the System Magnesium-Zinc", Kinzoku-no-Kenkyo, Japan Inst. of Metals, 6 (1929), p. 177.

6. K. P. Anderko, E. J. Klimek, D. W. Levinson, and W. Rostoker, "Constitution Studies on the System Magnesium-Zinc", Trans. of and A.S.M., 49 (1957), pp. 778-793.

7. J. B. Clark and F. N. Rhines, "Central Region of the Mg-Zn Phase Diagram", J. of Metals, 9 (1957), pp. 425-430.

8. W. Köster, and F. Müller, "The Ternary System Copper-Zinc-Magnesium", Zeit. für Metallkunde, 39 (1948), p. 352.

9. W. Köster, "Decomposition of the Mg_7Zn_3 Phase", Zeit. für Metallkunde, 41 (1950), p. 37.

10. H. D. Brody, M. C. Flemings, "Solute Redistribution in Dendrite Solidification", submitted to A.I.M.E. for publication.

11. M. Cohen, private communication, Massachusetts Institute of Technology, Cambridge, Massachusetts.

12. A. Papapetrou, "Untersuchungen über Dendritisches Wachstum von Kristallen", Zeit. für Kristallographie, 92 (1935), pp. 89-130.

13. A. A. Chernov, "Analysis of the Transformation Time of Dendritic Crystals and Interdendritic Liquid Inclusions", Kristallografiia, 1 (1956), pp. 583-588.

14. M. O. Klia, "On the Mechanism of Transformation of Dendritic Crystals", Kristallografiia, 1 (1956), pp. 577-582.

15. K. A. Jackson, J. D. Hunt, D. T. Uhlmann, and T. P. Seward, "The Equiaxed Zone in Castings", Trans. Met. Soc. A.I.M.E., 236 (1966), pp. 149-158.

16. T. Z. Kattamis and M. C. Flemings, "Solidification of Iron Base Alloys at Large Degrees of Undercooling", U.S. Army Materials Research Agency, Contract No. DA-19-020-SMC-0231(X), Interim Report, October 1965 - September 30, 1966 (to be published).

17. C. Hurlbut, "An Electric Counter for Thin Section Analysis", Amer. Jourl. Sci., 237 (1939), p. 253.

18. R. T. Howard and M. Cohen, "Quantitative Metallography by Point-Counting and Lineal Analysis", Trans. A.I.M.E., 72 (1947), pp. 413-426.

19. B. Chalmers, Principles of Solidification, John Wiley, 1964.

TABLE I

Plate Castings

Casting No.	Type	Alloy
1	Unchilled	Not grain refined
2	End chilled	Not grain refined
3	Unchilled	Grain refined
4	End chilled	Grain refined
5	Unchilled, quenched at 340°C	Not grain refined

TABLE II

Experimental Data from Magnesium-Zinc Alloy Test Castings

Plate Number	Measured Solidification Time t_f (sec.)	Arm Spacing or Grain Size d (μ)	$\eta \times 10^{-6}$ (cm^2/sec)	Eutectic Measured (wt %)	Grain Refinement	Casting Type
1	73	40	5	6.6	No	End chilled plate
1	438	85	6.7	5.1	No	End chilled plate
2	840	108	7.9	4.1	No	Unchilled plate
2	985	110	8.9	2.9	No	Unchilled plate
2	1278	115	10.5	2.7	No	Unchilled plate
2	1460	120	11.1	2.4	No	Unchilled plate
5	656	100	7.1	-	No	Sand casting-quenched at T_E
5	765	107	7.3	4.8	No	Sand casting-quenched at T_E
5	840	110	7.9	4.5	No	Sand casting-quenched at T_E
5	1278	125	9.5	3.3	No	Sand casting-quenched at T_E
-	1.8	6.5			No	Small sample cast against chill
-	4.6	10			No	Small sample cast against chill
3	146	50	6.4	2.8	Yes	End chilled plate
3	292	68	6.9	1.8	Yes	End chilled plate
3	547	82	8.9	-	Yes	End chilled plate
4	711	90	9.6	1.8	Yes	Unchilled plate
4	785	95	9.6	1.9	Yes	Unchilled plate
4	1080	110	9.8	-	Yes	Unchilled plate
-	32.9	26			Yes	Small sample cast against chill

Note: Solidification times were calculated assuming constant cooling rate, β, where the β used was the measured average cooling rate for the first 80 per cent of solidification. Solidification time, t_f, was then determined from $t_f = (T_L-T_E)/\beta$ where T_L and T_E are liquidus and eutectic temperatures, respectively.

TABLE III

Constants Used for Calculation of $\bar{M}$, Magnesium-Zinc Alloys

$\sigma = 1.8 \times 10^{-6}$ cal/cm^2

$H = -154$ cal/cm^3

$D_L = 5 \times 10^{-5}$ cm^2/sec

$m_L = -4.1$ °K/%

$k = 0.168$

Note: The value for σ was calculated for a close-packed face, assuming surface energy per atom equal to 0.45 heat of fusion per atom (see Chalmers[19], p. 73).

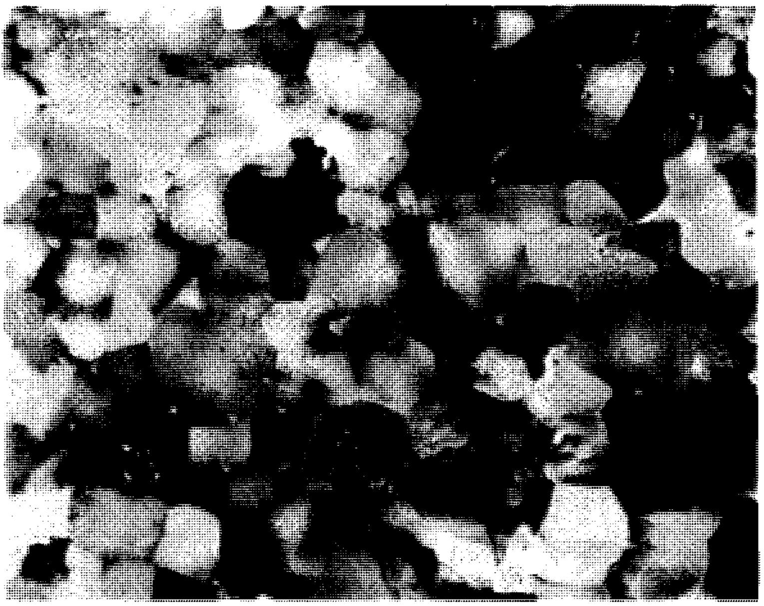

Figure 1: Microstructure of aluminum-4.5 per cent copper alloy slowly solidified with vibrating chill rod. Solidification time 12 hours; quenched from just below eutectic. Magnification 25X.

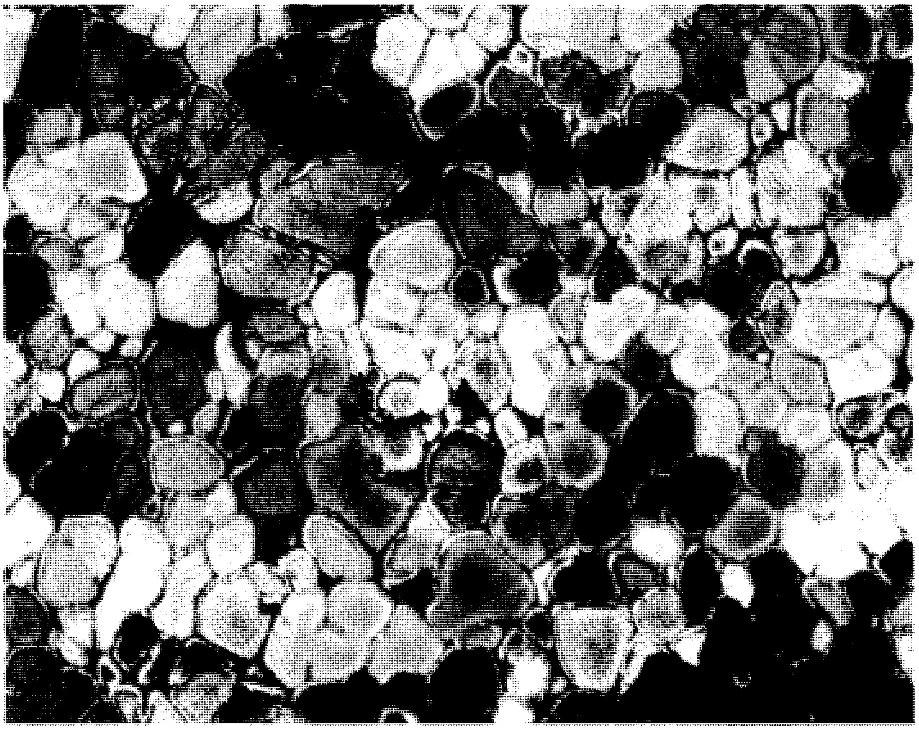

Figure 2: Microstructure of 7075 aluminum alloy slowly solidified with vibrating chill rod. Solidified approximately 25 per cent in three hours and water quenched. Magnification 50X.

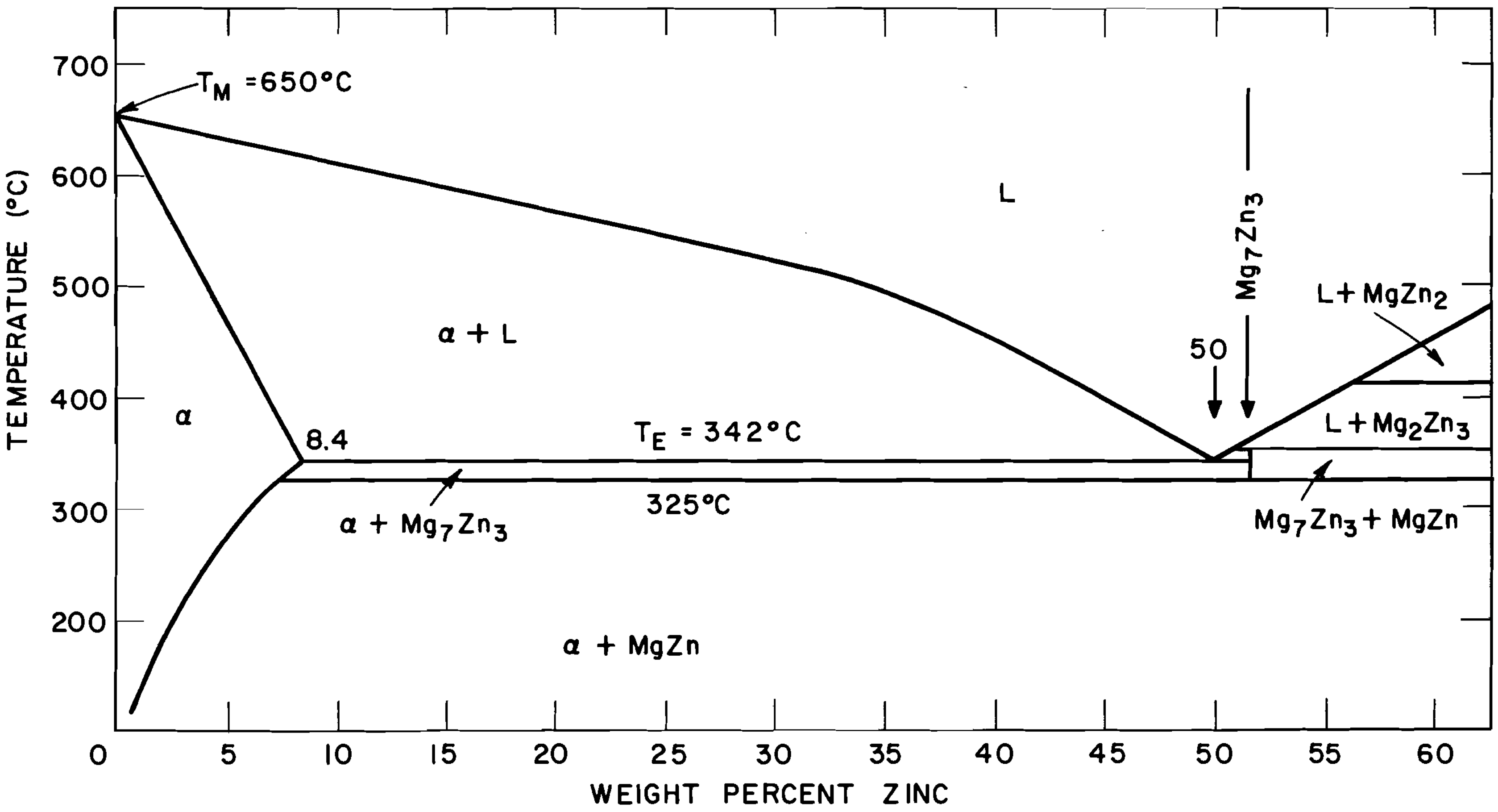

Figure 3: Phase diagram of the magnesium-zinc system (J. B. Clark and F. N. Rhines, Journal of Metals, 9, 1957, p. 425).

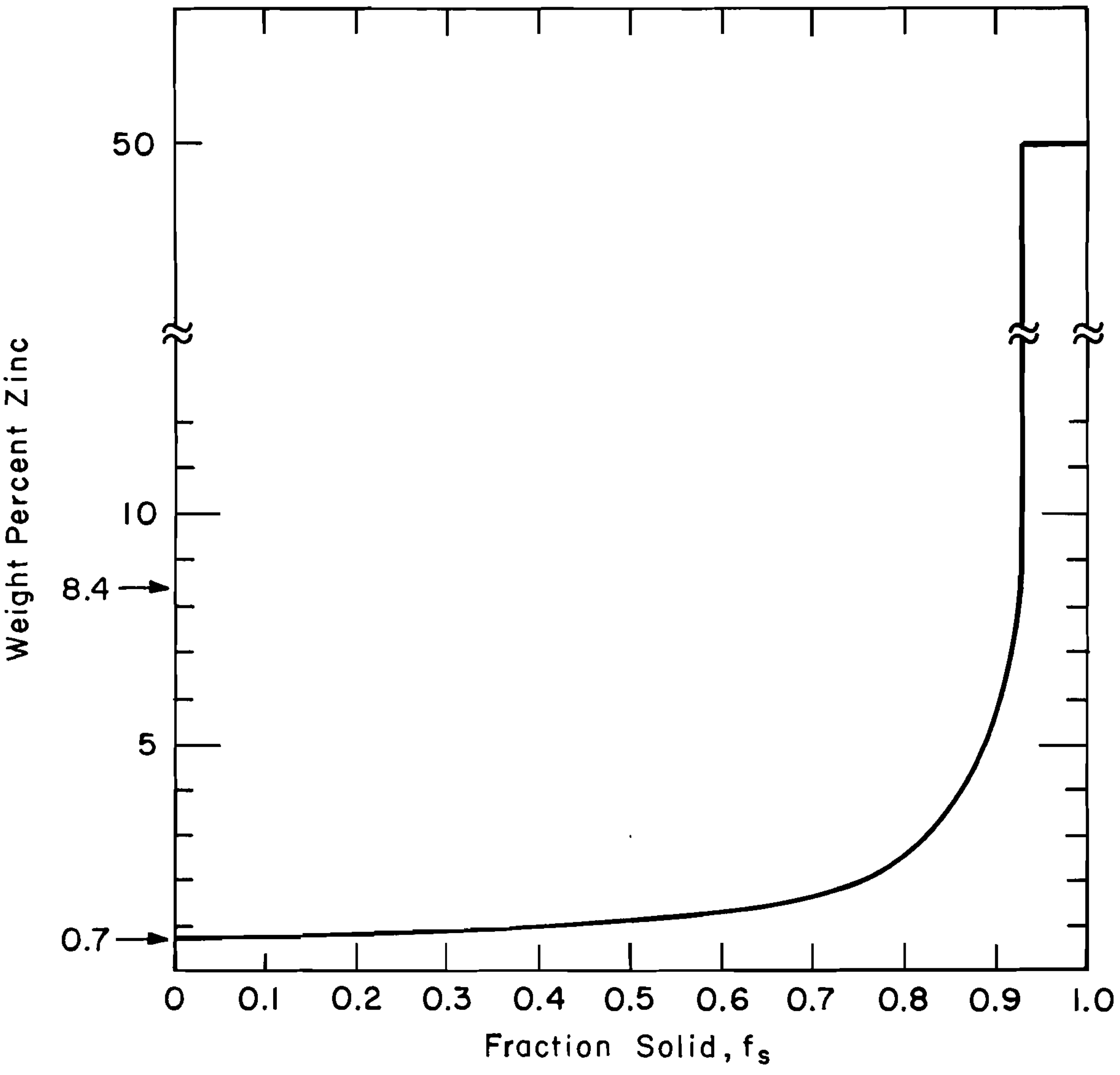

Figure 4: Solid composition versus fraction solid, assuming no solid diffusion, magnesium -5.5 per cent zinc.

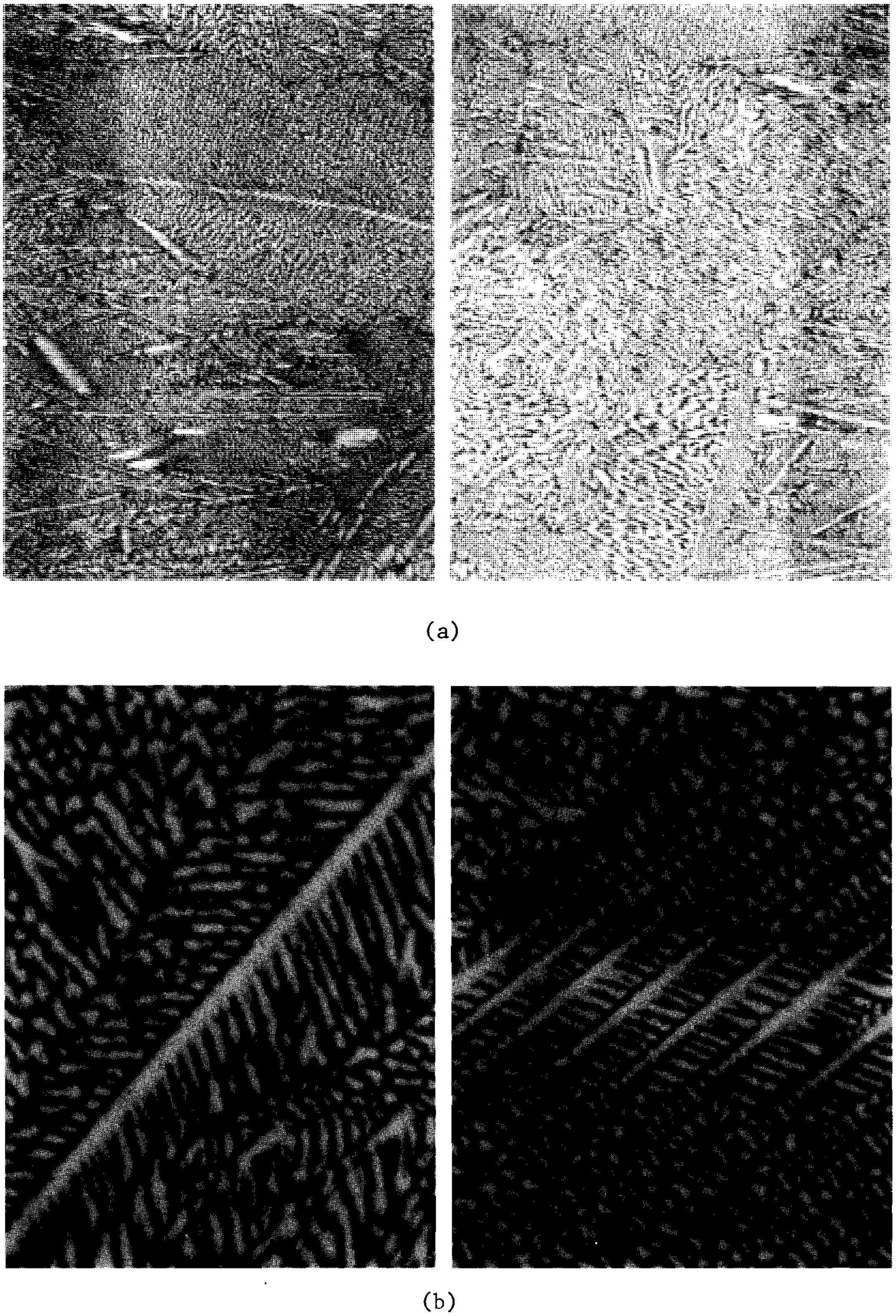

Figure 5: Microstructure of dendritic magnesium-zinc alloy. Solidification time, 0.5 seconds; arm spacing, 6.5 microns. (a) Magnification 55X. (b) Magnification 310X.

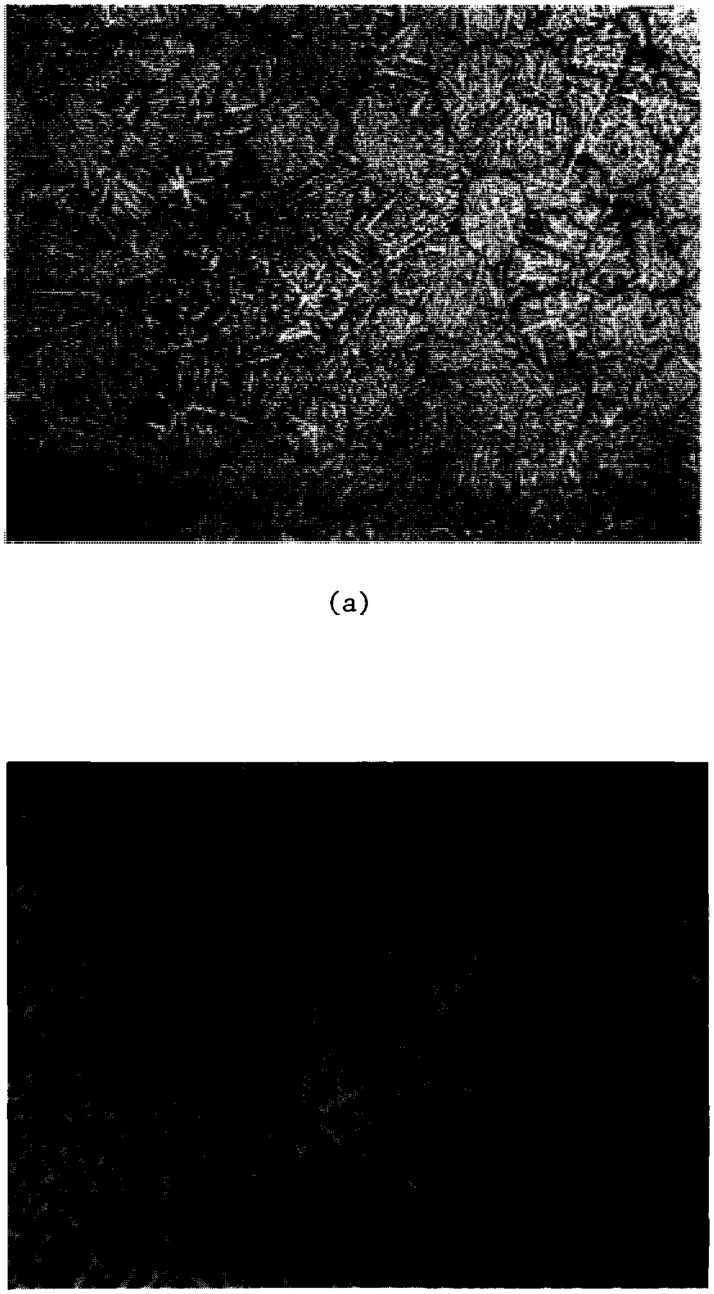

(a)

(b)

Figure 6: Microstructure of dendritic magnesium-zinc alloy. Solidification time, 20 seconds; arm spacing, 40 microns. (a) Magnification 12X. (b) Magnification 55X.

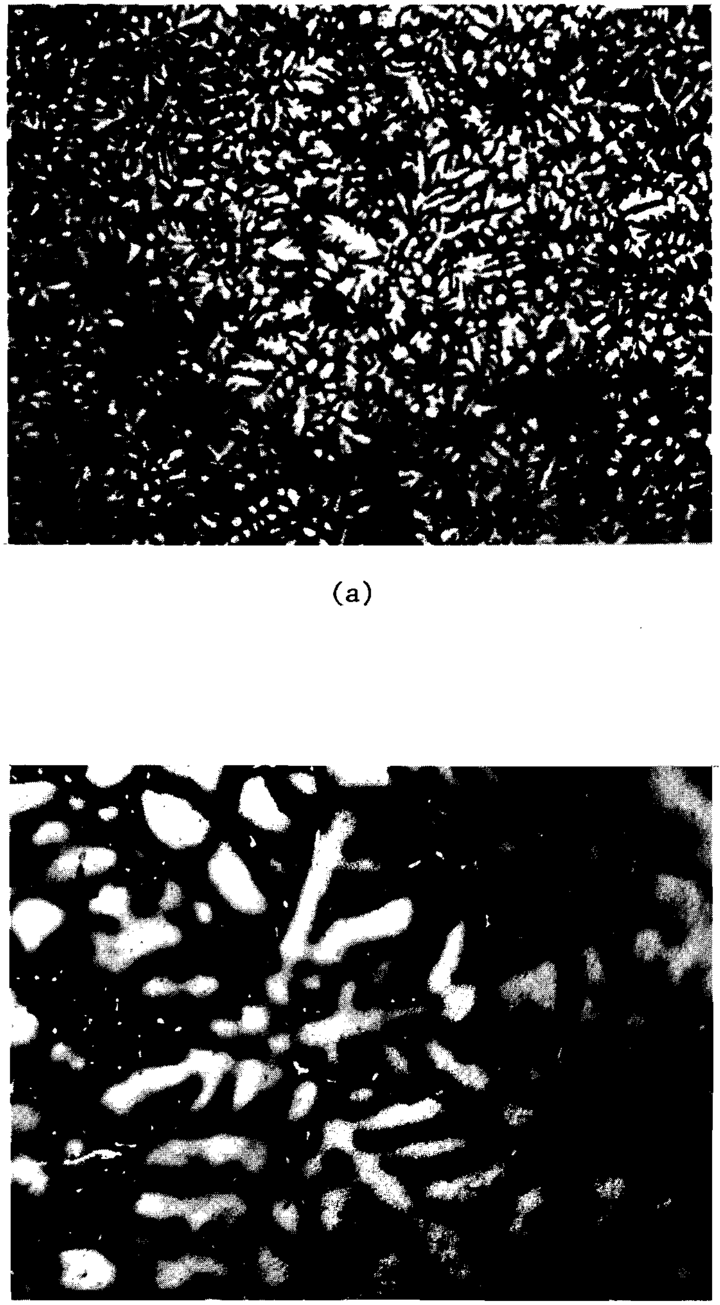

(a)

(b)

Figure 7: Microstructure of dendritic magnesium-zinc alloy. Solidification time, 120 seconds; arm spacing, 85 microns. (a) Magnification 12X. (b) Magnification 55X.

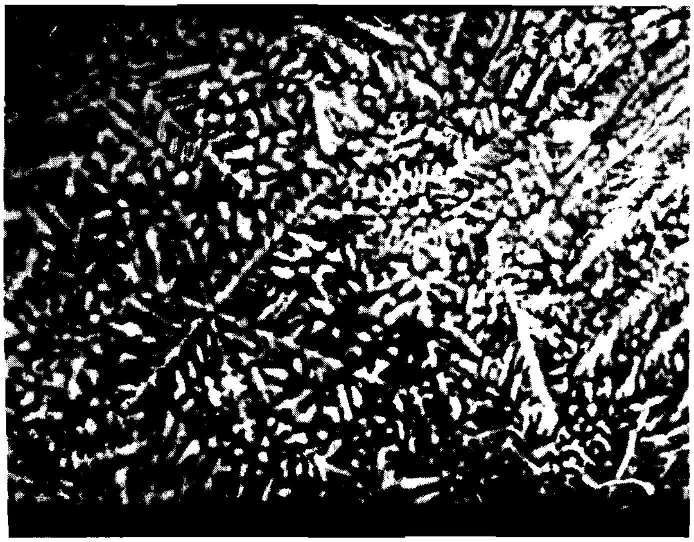

(a)

(b)

Figure 8: Microstructure of dendritic magnesium-zinc alloy. Solidification time, 350 seconds; arm spacing, 120 microns. (a) Magnification 12X. (b) Magnification 55X.

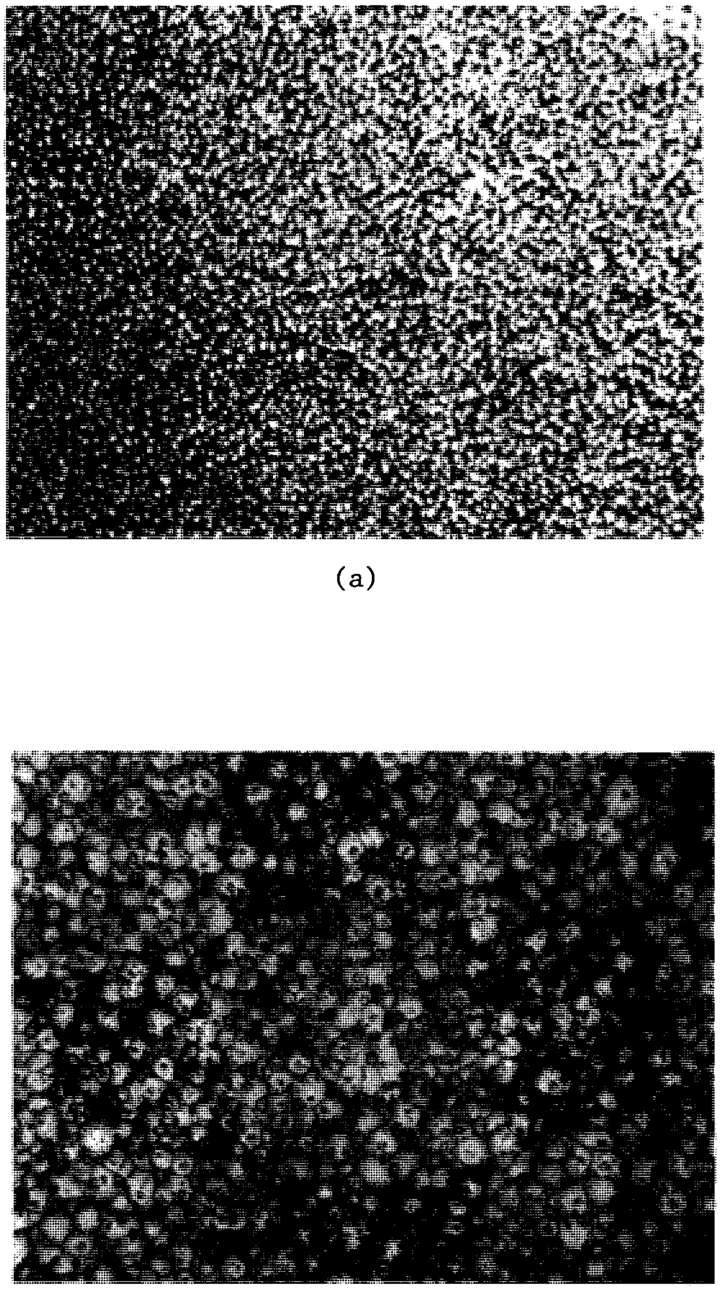

(a)

(b)

Figure 9: Microstructure of grain refined magnesium-zinc alloy; magnification 55X. (a) Solidification time, 9 seconds; grain size, 26 microns. (b) Solidification time, 100 seconds; grain size, 73 microns.

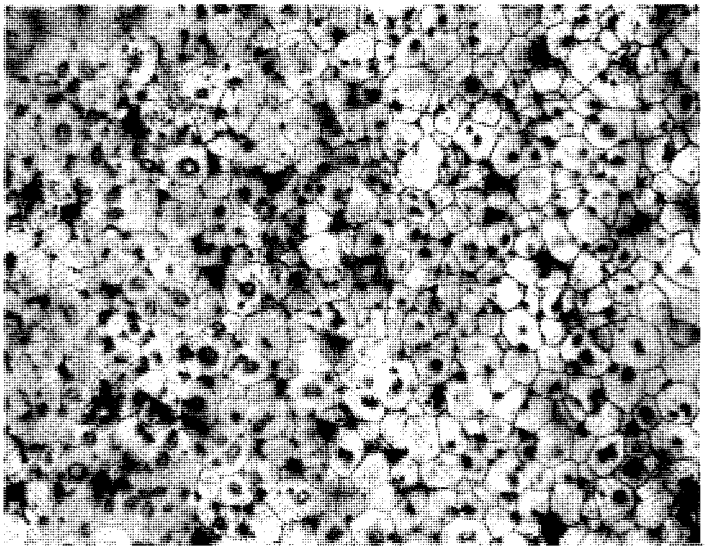

(a)

(b)

Figure 10: Microstructure of grain refined magnesium-zinc alloy; magnification 55X. (a) Solidification time, 420 seconds; grain size, 105 microns. (b) Solidification time, 550 seconds; grain size, 111 microns.

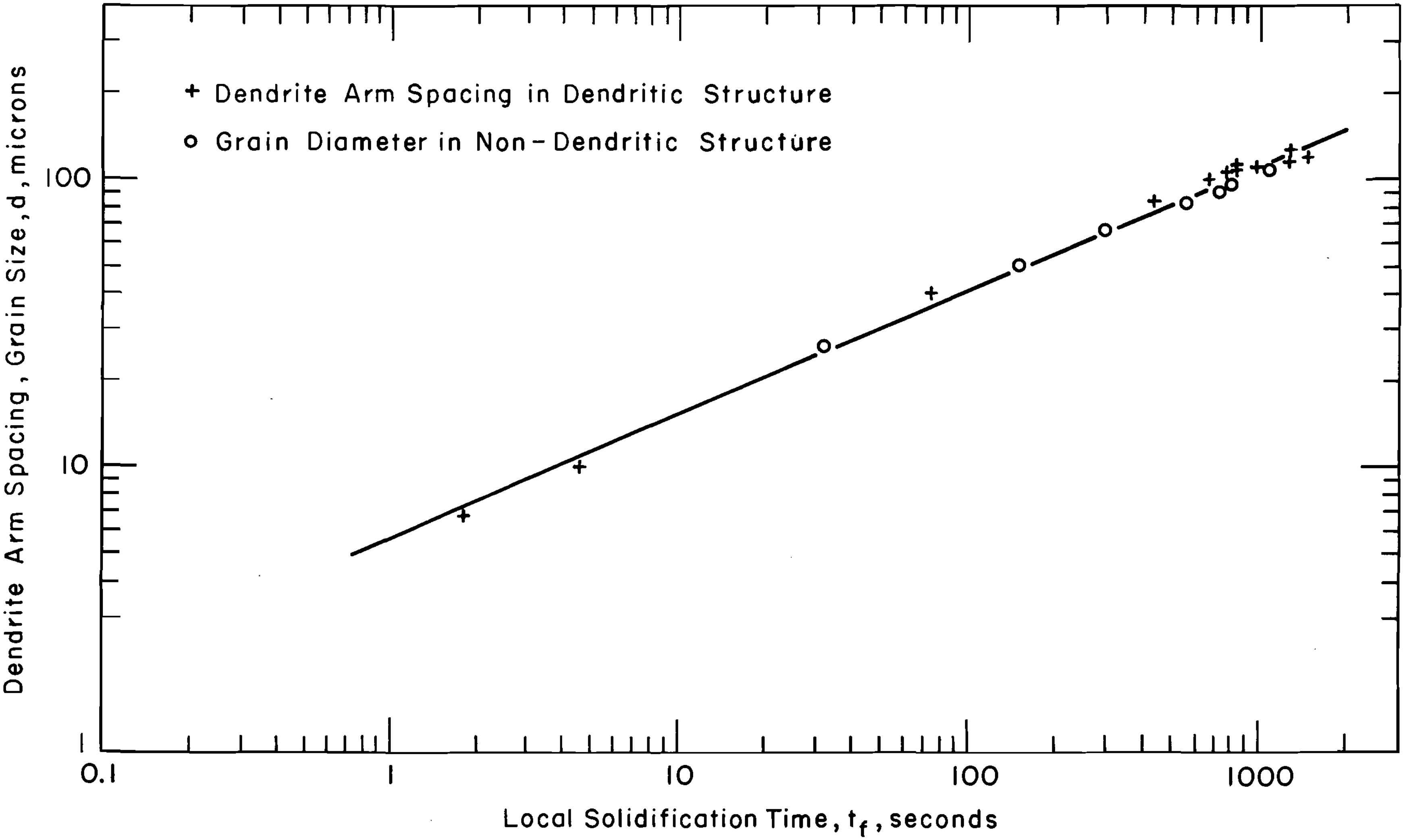

Figure 11: Dendrite element spacing versus solidification time in dendritic and non-dendritic magnesium-5.5 per cent zinc alloy.

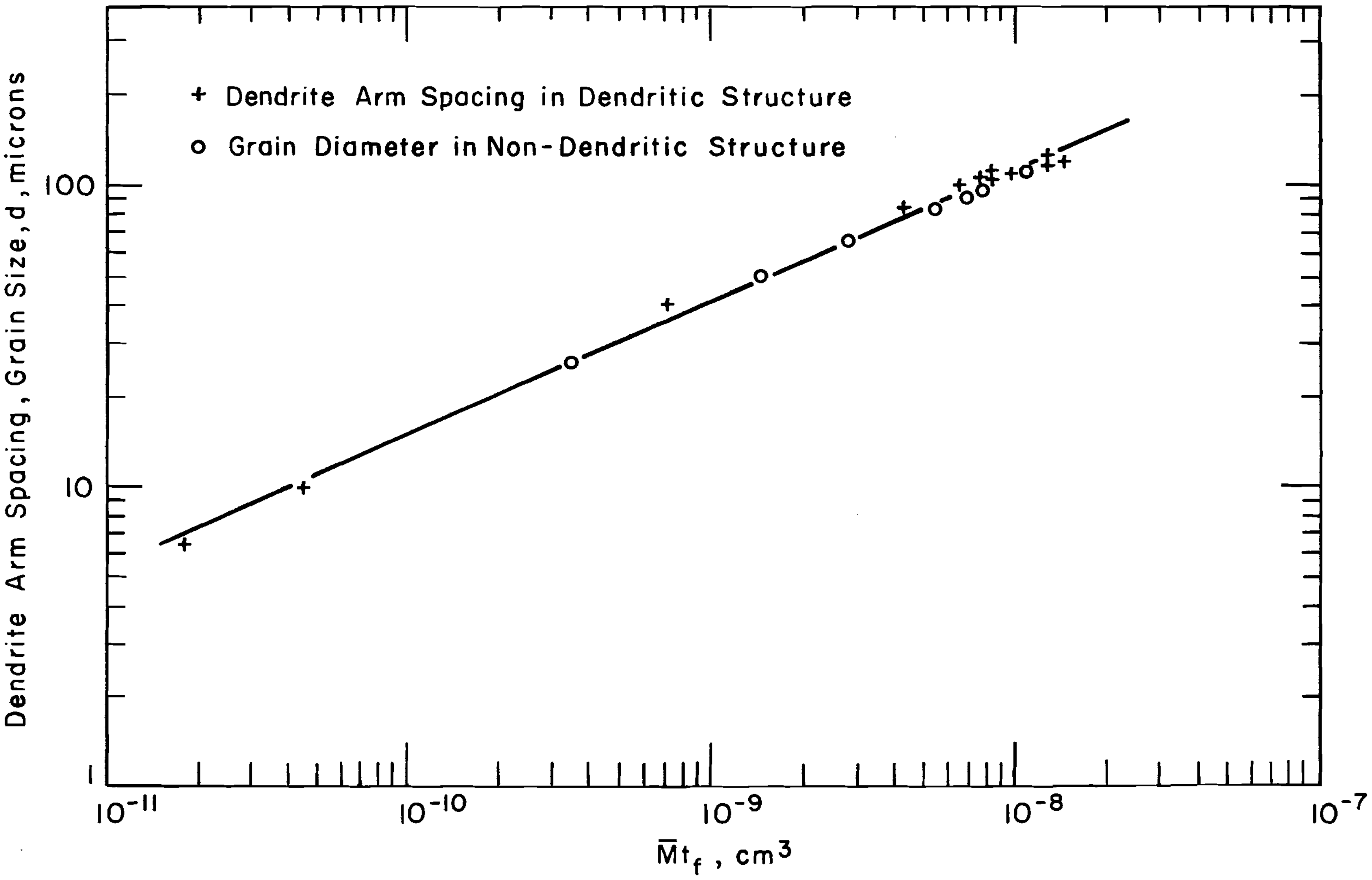

Figure 12: Dendrite arm spacing, d, versus $\bar{M}t_f$, magnesium-5.5 per cent zinc alloy.

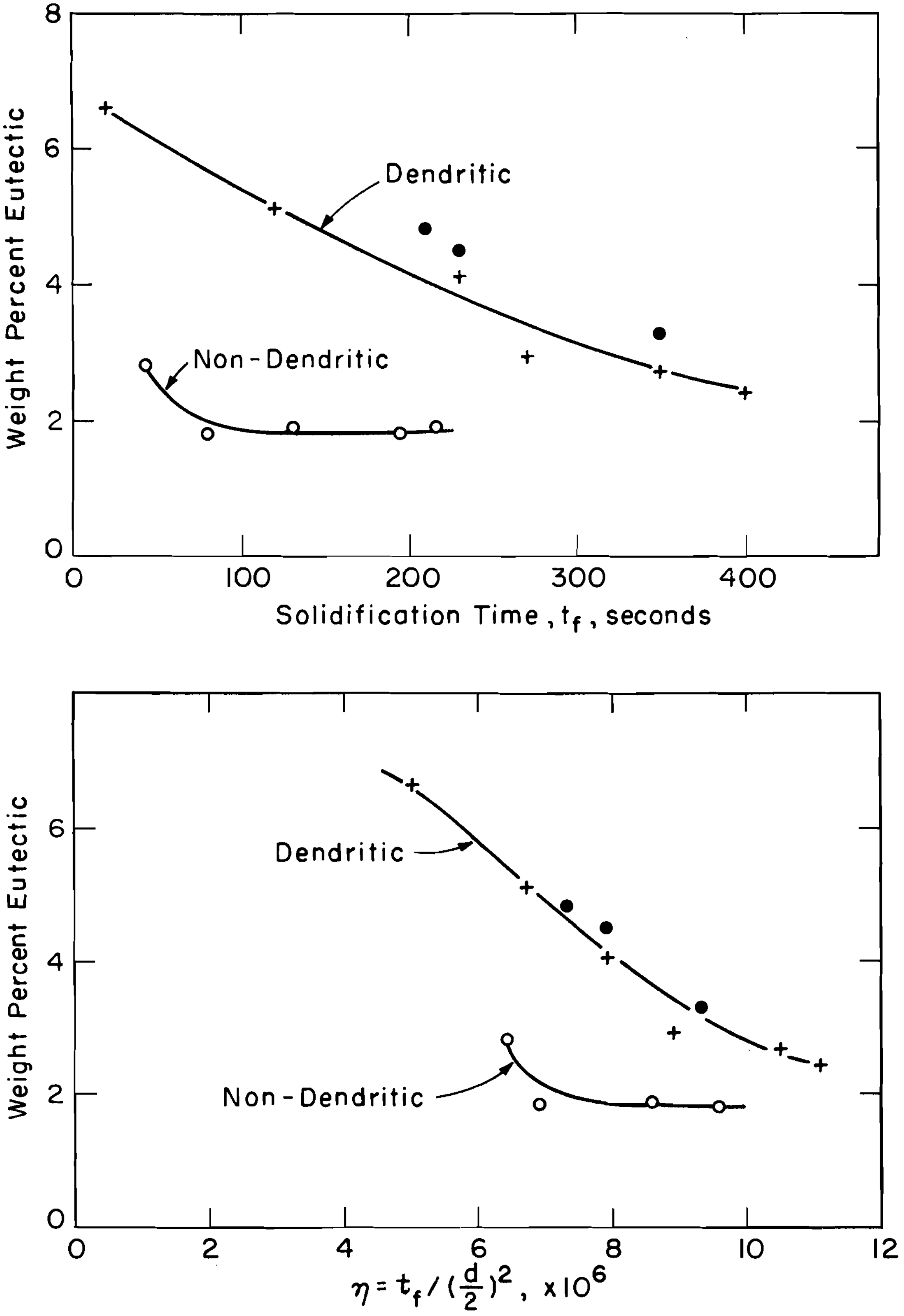

Figure 13: Weight per cent eutectic versus solidification time (top) and η (bottom); dendritic specimens.

\+ not quenched, dendritic
● quenched from just below eutectic, dendritic
o non-dendritic

Chapter 6: PREDICTIONS OF DENDRITE ARM SPACING IN ALUMINUM ALLOYS

ABSTRACT

Experimental data on dendrite arm spacings in aluminum-copper alloys are compared with an analysis based on coarsening kinetics. Arm spacings are shown to depend only on the quantity $\bar{M}t_f$ ($\bar{M}$ = coarsening parameter, t_f = solidification time) for a wide range of alloy analyses and solidification times. The engineering importance of the agreement found is that for the first time:

(1) It appears the mechanism controlling final dendrite arm spacing in castings and ingots has been established,

(2) It should be possible to correlate experimental measurements on dendrite arm spacings from different alloys and different alloy systems, and

(3) It should be possible to predict at least semi-quantitatively the influence of alloy variations or other process variables on dendrite arm spacing.

A. Introduction

Work reported in the previous chapter illustrated the dependence of dendrite arm spacing on coarsening phenomena; a similar dependence was shown for grain size in non-dendritic melts. Detailed consideration is given in this chapter to effect of coarsening in determining dendrite arm spacing of aluminum alloys. Arm spacing is first examined in aluminum-copper alloys held isothermally above the non-equilibrium solidus; it is shown this spacing increases with time according to coarsening kinetics. It is then illustrated that dendrite arm spacing in aluminum-copper alloys solidified in usual ways also obeys a simple coarsening law. Finally, it is shown that a simple analysis is able to predict, for the first time, effects of alloy elements on dendrite arm spacing in aluminum base alloys.

B. Isothermal Coarsening

In order to illustrate effect of coarsening on dendrite arm spacing, a series of isothermal experiments were performed in the following way. Small samples were taken from an air-cooled unidirectionally solidified aluminum-4.5 per cent copper alloy ingot. Samples were from a location 7 inches from the chill; these had an initial solidification time of 9300 seconds and initial secondary dendrite arm spacing of 300 microns.

The samples were heated to 635°C, at which temperature they were approximately 50 per cent liquid[1,2]. They were held at this temperature for varying lengths of time, up to ten times the original freezing time, and were then water quenched.

Microstructures of a series of the samples are shown in Figures 1 through 4. Figure 1 shows the original, as-cast, structure, and Figures 2 through 4 show how the coarsening rapidly takes place during isothermal holding, with finer dendrite arms disappearing and material from these arms reprecipitating on the few remaining arms. Final, average dendrite arm spacings for the four specimens shown in Figures 1 through 4 are superimposed on a graph (Figure 5) of dendrite arm spacing versus solidification time, t_f. The times, t_f, used to plot the data from the isothermally held specimens are the original solidification times (9300 seconds for all samples) plus isothermal holding times. These holding times are listed in Figures 1 through 4 for the structures shown.

The structures of Figures 1 through 4 are clear proof that coarsening kinetics controls final dendrite arm spacing in these isothermal experiments. Moreover, as shown by Figure 5, increasing isothermal holding time has a quantitatively similar effect on dendrite arm spacing as does increasing solidification time. Hence, the experiments are strongly suggestive that dendrite arm spacing in usual solidification processes is determined by the same mechanism; i.e., by coarsening.

C. Solidification Experiments

In the previous chapter, an approximate expression was given to relate dendrite arm spacing to solidification time, derived by Kattamis and Flemings elsewhere[3]. A brief summary derivation is given in Appendix A. The equation is:

$$d = A\,(\bar{M}t_f)^n \qquad (1)$$

where:

$$\bar{M} = \frac{2\sigma D_L T_L \ln \frac{C_E}{C_o}}{H(1 - k)m_L(C_E - C_o)} \qquad (1a)$$

d = average final dendrite element spacing*, cm

t_f = solidification time, sec

σ = liquid-solid surface energy, cal/cm^2

D_L = liquid diffusion coefficient, cm^2/sec

T_L = equilibrium liquidus temperature, °K

H = volumetric heat of fusion, cal/cm^3

C_E = eutectic composition, weight per cent

C_o = initial liquid composition, weight per cent

k = equilibrium partition ratio, dimensionless

m_L = liquidus slope (°K/%)

A, n = constants

Equation (1) predicts that dendrite arm spacing should depend directly on $\bar{M}$, t_f, and two constants. $\bar{M}$ is dependent only on properties of the metal (heat of fusion, alloy analysis, etc.). If, then, the constants A and n are determined by either analysis or experiment, equation (1) provides an excellent engineering basis on which to correlate experimental results on dendrite arm spacings, and to predict effects of alloy elements on this spacing.

---

* "Dendrite element spacing" is defined as dendrite arm spacing in dendritically solidifying melts and grain diameter in non-dendritic structures.

The engineering importance of the foregoing, and particularly of equation (1) is that for the first time:

(1) It appears the mechanism controlling final dendrite arm spacing in casitngs and ingots has been established,

(2) It should be possible to correlate experimental measurements on dendrite arm spacings from different alloys and different alloy systems, and

(3) It should be possible to predict as least semi-quantitatively the influence of alloy variations or other process variables on dendrite arm spacing.

To illustrate the above, data of Horwath and Mondolfo[4] have been compared with predictions of equation (1). Horwath and Mondolfo[4] conducted a detailed study of effects of cooling rate and alloy analysis on dendrite arm spacing in aluminum-copper alloys. Results are summarized in Figure 6.

Using the constants of Table I, $\bar{M}$ and t_f have been calculated for each of the points in Figure 6 and d plotted versus $\bar{M}t_f$ (on logarithmic scale, Figure 7). For these alloys, varying in composition from 0 to 22 atomic per cent copper (0 to 40 weight per cent), and in cooling rates from 0.1°C/min to 1000°C/min, all data lie, with very little scatter about a straight line described by equation (1), with a slope, n, equal to 0.25. All the data points of Figure 6 are included in

Figure 7 from both the hypo- and by hyper-eutectic alloys. The agreement between experiment and analysis by outstanding.

For comparison with the foregoing, the data of Figure 5 for aluminum-4.5 per cent copper replotted as log d versus log $\bar{M}t_f$ in Figure 8.

The straight line drawn through the points in Figure 8 corresponds directly to the straight line drawn through the original experimental data, in Figure 5; the slope of both lines is the same, n = 0.39. This slope is somewhat greater than that of the line drawn through the data of Horwath and Mondolfo, Figure 7, where n = 0.25. However, comparison of the actual data of Figures 7 and 8 shows exact agreement within the limits of experimental scatter. The agreement between experiment and analysis is again outstanding.

For final comparison, compare Figure 12 of Chapter 5 with Figures 7 and 8 of this chapter. Figure 12 plots d versus $\bar{M}t_f$ for dendritic and non-dendritic magnesium-zinc alloy. In all three curves, identical relations for d versus $\bar{M}t_f$ are obtained, within uncertainties of experimental error and of numerical values employed for the various constants. The conclusion is clear, that for all the non-ferrous alloys studied, dendrite arm spacing depends only on solidification time and the parameter, $\bar{M}$.

D. Conclusions

1. Within the limits of experimental error, dendrite arm spacing, d, in a variety of aluminum-copper alloys has been found to depend only on solidification time, t_f, and a coarsening parameter $\bar{M}$.

2. Within the limits of experimental error, the relation obtained for d versus $\bar{M}t_f$ for aluminum-copper alloys is the same as that for a magnesium-zinc alloy, and the relation is therefore presumed to be of general applicability for non-ferrous alloys.

3. The engineering importance of the foregoing, is that for the first time:

(a) It appears the mechanism controlling final dendrite arm spacing in castings and ingots has been established,

(b) It should be possible to correlate experimental measurements on dendrite arm spacings from different alloys and different alloy systems, and

(c) It should be possible to predict at least semiquantitatively the influence of alloy variations or other process variables on dendrite arm spacing.

REFERENCES

1. "Effects of Solidification Variables on the Structure of Aluminum Base Ingots", Casting and Solidification Section, M.I.T., Department of Army, Material Command, MUCOM, Frankford Arsenal, Philadelphia, Pa., under Contract No. DA-19-020-ORD-5706(A), June 1963 - June 1964.

2. H. D. Brody and M. C. Flemings, "Solute Redistribution in Dendritic Solidification", submitted for publication, Trans. Met. Soc. A.I.M.E.

3. T. Z. Kattamis and M. C. Flemings, "Solidification of Iron Base Alloys at Large Degrees of Undercooling", U.S. Army Materials Research Agency, Contract No. DA-19-020-ORD-SMC-0231(X), Interim Report, October 1965 - September 30, 1966 (to be published).

4. J. A. Horwath and L. F. Mondolfo, "Dendritic Growth", Acta Met., Vol. 10 (1962), pp. 1037 - 1042.

5. T. F. Bower, H. D. Brody and M. C. Flemings, "Measurements on Solute Redistribution in Dendritic Solidification", submitted for publication, Trans. Met. Soc. A.I.M.E.

6. C. Wagner, "Theorie der Alterung von Niederschlagen durch Umlosen", Zeit. fur Elektrochemie, 1961, Vol. 65, No. 78, pp. 581-591.

7. A. E. Nielsen, <u>Kinetics of Precipitation</u>, Pergamon Press, Ltd., Oxford, 1964.

8. B. Chalmers, <u>Principles of Solidification</u>, John Wiley, 1964.

TABLE I

Constants for Aluminum-Copper Alloys Used in Calculations of d versus t_f

$\sigma = 1.2 \times 10^{-6}$, cal/cm^2

$H = -250$, cal/cm^3

$D_L = 5 \times 10^{-5}$, cm^2/sec

$m_L = -3.33$, °C/%
$k = 0.18$
for $0\% < C_o < 33\%$

$m_L = -1.72$, °C/%
$k = 0.75$
for $33\% < C_o < 40\%$

TABLE II

Data from Horwath and Mondolfo[4], and Calculated Values of t_f and $\bar{M}$

C* (wt % copper)	β* (°C/min)	d* cm x 10^4	t_f** (sec)	$\bar{M}^+$ cm^3/sec
5	0.1	350	5.82×10^4	1.2×10^{-11}
10	0.1	280	4.92	0.832
15	0.1	190	4.07	0.691
20	0.1	150	2.82	0.59
25	0.1	125	1.62	0.52
30	0.1	110	0.48	0.46
35	0.1	120	0.12	1.28
40	0.1	140	0.72	1.45
5	1	140	5.82×10^3	1.2×10^{-11}
10	1	130	4.92	0.832
15	1	95	4.07	0.691
20	1	85	2.82	0.59
25	1	70	1.62	0.52
30	1	58	0.48	0.46
35	1	58	0.12	1.28
40	1	72	0.72	1.45
5	10	80	5.82×10^2	1.2×10^{-11}
10	10	70	4.92	0.832
15	10	56	4.07	0.691
20	10	46	2.82	0.59
25	10	38	1.62	0.52
30	10	30	0.48	0.46
35	10	30	0.12	1.28
40	10	42	0.72	1.45

TABLE II (cont'd)

C* (wt % copper)	β* (°C/min)	d* cm x 10^4	t_f** (sec)	$\bar{M}$+ cm^3/sec
5	100	40	58.2	1.2×10^{-11}
10	100	35	49.2	0.832
15	100	30	40.7	0.691
20	100	24	28.2	0.59
25	100	19	16.2	0.52
30	100	15.5	4.8	0.46
35	100	12	1.2	1.28
40	100	21	7.2	1.45
5	1000	18	5.82	1.2×10^{-11}
10	1000	17	4.92	0.832
15	1000	15	4.07	0.691
20	1000	13	2.82	0.59
25	1000	12	1.62	0.52
30	1000	8	0.48	0.46
35	1000	4.4	0.12	1.28
40	1000	9	0.72	1.45

---

* Data from Horwath and Mondolfo[4]. For calculation of $\bar{M}$ for hypereutectic alloys, weight per cents employed were 100 - C_o.

** Calculated assuming constant β over the solidification range.

\+ Calculated using constants of Table I.

APPENDIX A

Summary Derivation of Equation (1)

The following is intended only as an outline of the derivation of the approximate relation, equation (1). Detailed derivation, by Flemings and Kattamis is given elsewhere[3].

Wagner[6] and Nielsen[7] give an expression for the mean radius of particles "ripening" in solution for various times t:

$$\bar{r}^3 = M't \tag{1}$$

where: $\bar{r}$ = arithmetic average particle radius

t = time

$M' = \dfrac{\sigma v^2 D_L C_L'}{kT}$

σ = surface energy, cal/cm^2

v = molecular volume, cm^3/mol

D_L = liquid diffusion coefficient, cm^2/sec

C_L' = liquid concentration, mol/cm^3

k = Boltzman's constant, cal/mol °C

T = absolute temperature, °K

Assumptions of equation (1) include:

(a) spherical particles of isotropic surface energy

(b) initial gaussian distribution of particle sizes

(c) non-overlapping diffusion fields

(d) no kinetic limitation to growth

(e) constant volume fraction solid

(f) no solid solubility

For solutions with some solid solubility, as metallic alloys, a more accurate and convenient expression is:

$$\bar{r}^3 = Mt \tag{2}$$

where

$$M = \frac{2\sigma D_L T_e}{HC_L^*(1 - k)m_L} \tag{2a}$$

H = volumetric heat of fusion, cal/cm^3

C_L^* = liquid concentration, weight per cent

k = equilibrium partition ratio

m_L = liquidus slope, °K/%

In solidification processes volume fraction solid is not, of course, constant. However, it is simply shown by examination of experimental data that the growth of those dendrite elements that finally survive comes overwhelmingly from "ripening"; the contribution from direct solidification is negligible. As a result, in spite of the fact that volume fraction solid is continually changing it is possible to write:

$$\bar{r}^3 \approx \int_o^t M dt \tag{3}$$

For the conditions of constant cooling rate, constant σ, D_L, H, k, m_L, and for $T \approx T_L$, it is readily shown that:

$$\bar{r}^3 \approx \bar{M}t \qquad (4)$$

where:

$$\bar{M} = \frac{2\sigma D_L T_L \ln \frac{C_E}{C_o}}{H(1 - k)m_L(C_E - C_o)} \qquad (4a)$$

Finally, at $t = t_f$, $\bar{r} = \frac{d}{2}$, and:

$$d \approx 2(\bar{M}t_f)^{1/3} \qquad (5)$$

where: d = dendrite element spacing (at end of solidification)

t_f = solidification time

Diffusion fields in the liquid do, however, strongly overlap during solidification of metallic alloys[1,2,5], and so assumption (c) above is not valid, particularly near the end of solidification. As a preliminary attempt at a more reasonable model, diffusion distance in the liquid was assumed proportional to $r^{(n-2)}$ where n is constant. The resulting expression is of the form of (5) but with different constants, i.e.,

$$d \approx A(\bar{M}t_f)^n \qquad (6)$$

where A and n are constants

It is equation (6) that is used for comparison of coarsening theory with experiment. Constants A and n are determined empirically.

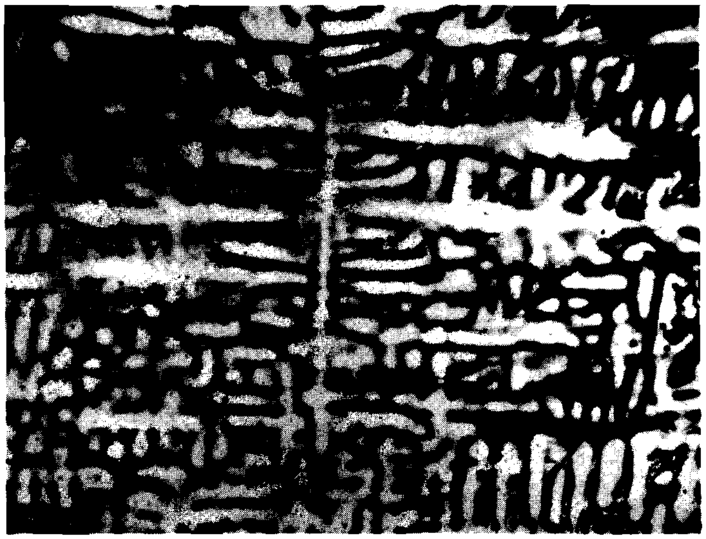

Figure 1: Microstructure of unidirectionally solidified aluminum-4.5 per cent copper alloy, t_f = .93 x 10^4 sec. As-cast structure, d = 200 microns. 12X.

Figure 2: Microstructure of samples of Figure 1, isothermally coarsened at 50 per cent solid for 1.08 x 10^4 sec., d $\approx$ 400 microns (d is spacing of coarsened structure). Fine structure is that resulting from water quenched. 12X.

Figure 3: Microstructure of sample of Figure 1, isothermally coarsened at 50 per cent solid for 2.52×10^4 sec., $d \approx 500$ microns (d is spacing of coarsened structure). Fine structure is that resulting from water quench. 12X.

Figure 4: Microstructure of sample of Figure 1, isothermally coarsened at 50 per cent solid for 9.0×10^4 sec., $d \approx 800$ microns (d is spacing of coarsened structure). Fine structure is that resulting from water quench. 12X.

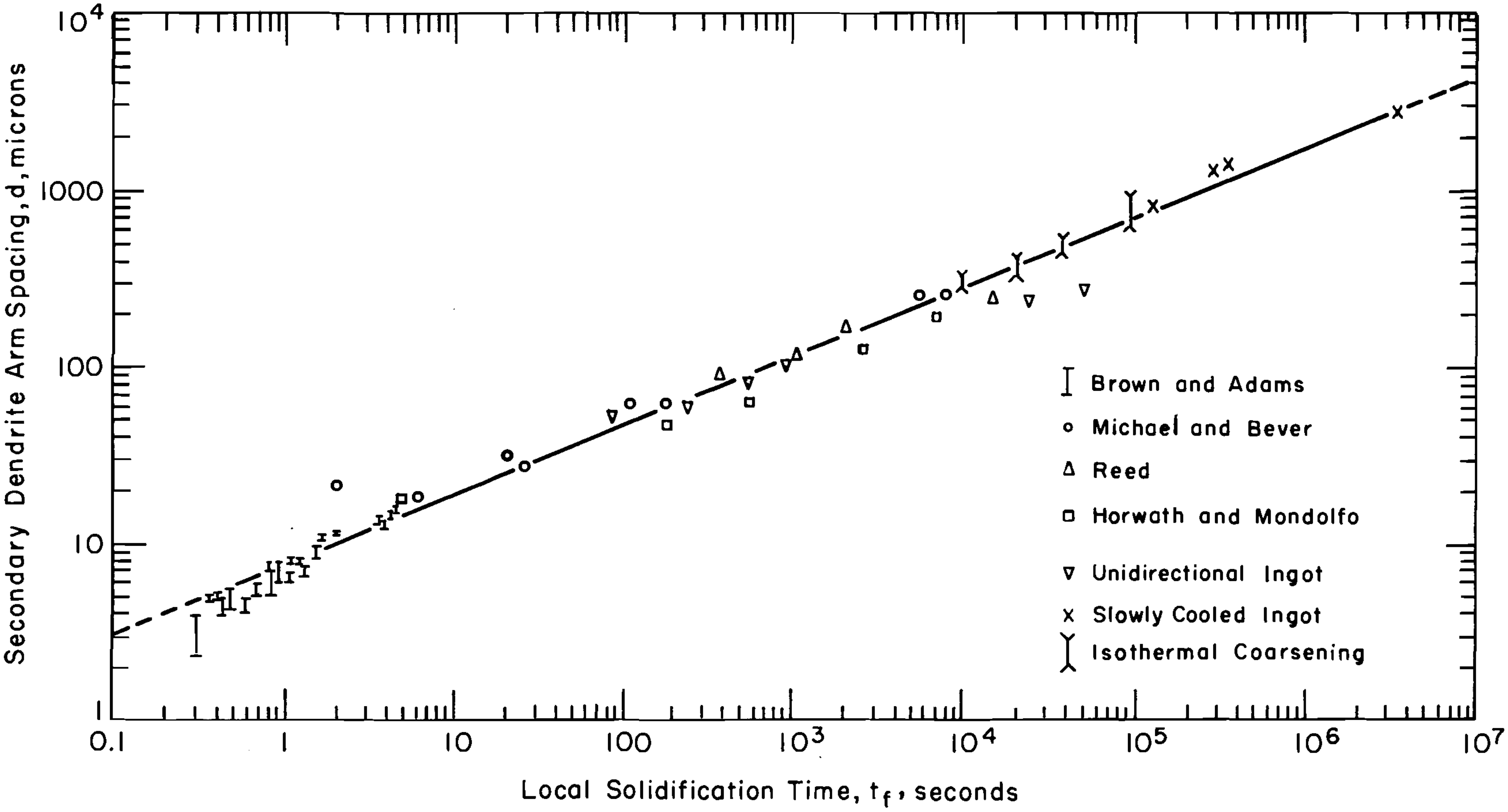

Figure 5: Dendrite arm spacing versus local solidification time for aluminum-copper alloys, as reported earlier[1,5]. Data for isothermal coarsening experiments are superimposed.

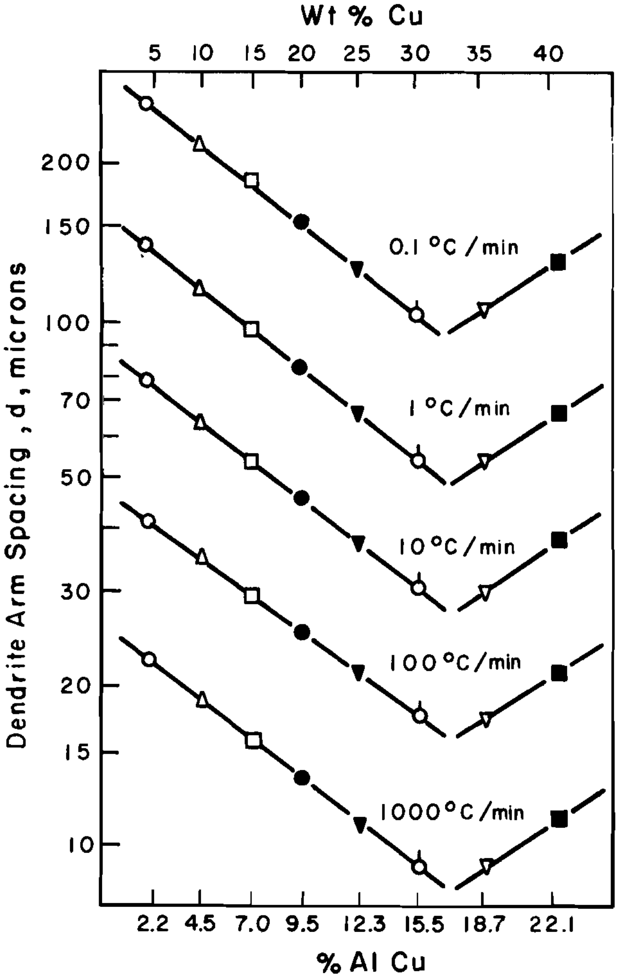

Figure 6: Dendrite arm spacing of aluminum-copper alloys as a function of copper content and cooling rate. (From Horwath and Mondolfo[4])

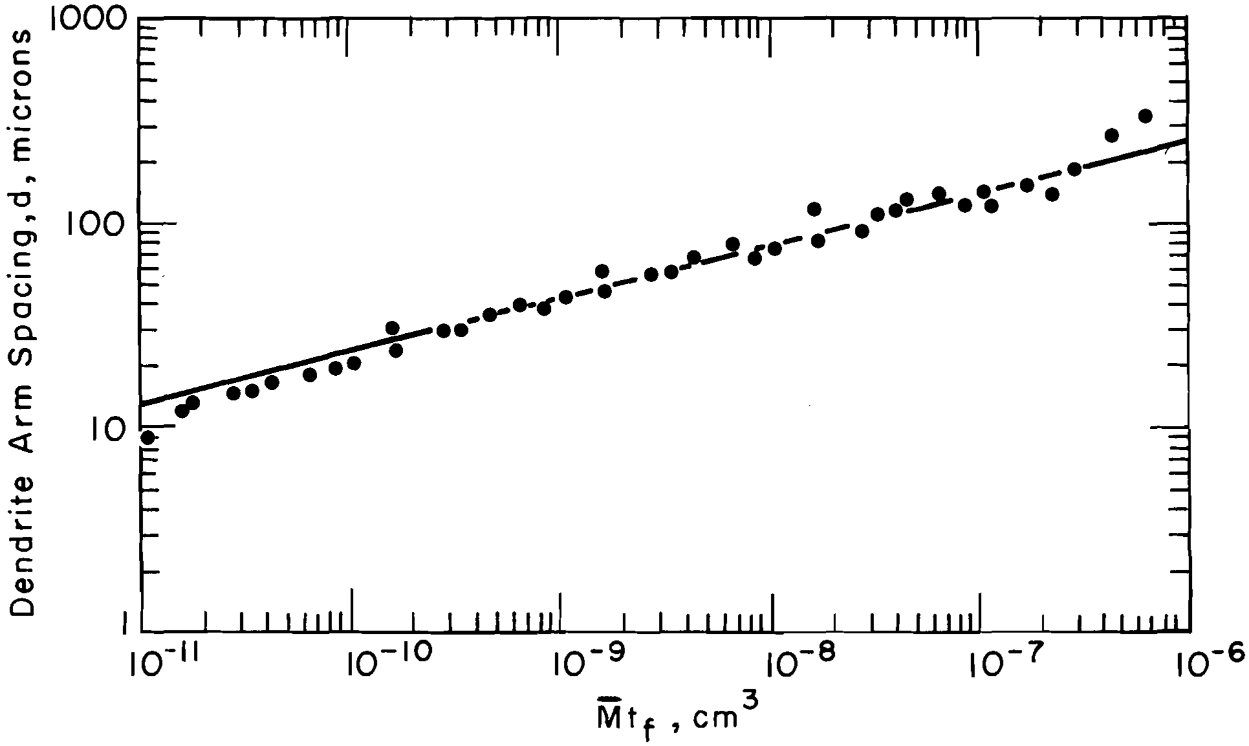

Figure 7: Dendrite arm spacing, d, versus $\bar{M}t_f$ for hypo- and hyper-eutectic aluminum-copper alloys. Data are for C_o in the range of 5 to 40 weight per cent copper and t_f in the range of .12 to 5.8 x 10^4 sec. Data from Horwath and Mondolfo, Figure 6.

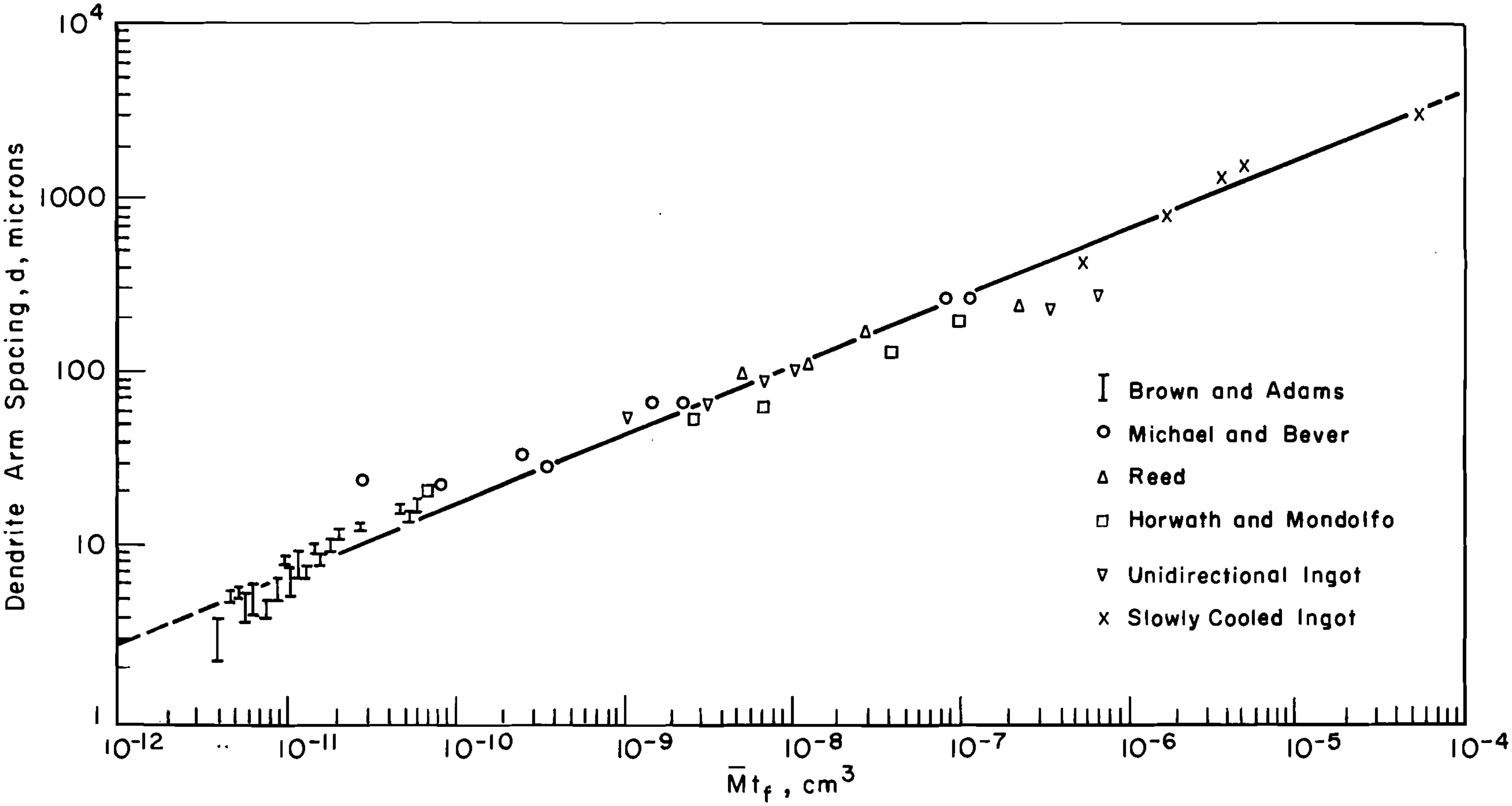

Figure 8: Dendrite arm spacing, d, versus $\bar{M}t_f$ for aluminum-copper alloys.

DISTRIBUTION LIST

Addressee	No. of Copies
HQ, U.S. Army Material Command	
Attn: AMCRD-RC-M	1
AMCRD-DM	1
AMCRD-DW	1
Washington, D. C. 20315	
HQ, U.S. Army Material Command	
Attn: AMSMU-LM	1
U.S. Marine Corps	
Liaison Officer	
Washington, D. C. 20315	
Commanding General	
U.S. Army Weapons Command	
Attn: AMSWE-RDR	1
Rock Island, Illinois, 61202	
Commanding Officer	
U.S. Army Ballistics Res. Labs.	1
Aberdeen Proving Ground	
Maryland 21005	
Commanding Officer	
U.S. Army Materials Research Agency	
Attn: PS & C Division	1
Watertown Arsenal	
Watertown, Mass. 01272	
Commanding Officer	
Picatinny Arsenal	
Attn: Technical Group	1
Dover, New Jersey 07801	
Commanding Officer	
Watertown Arsenal	
Attn: Library	1
Mr. G. Darcy	1
Mr. J. P. Jones	1
Watertown, Mass. 02172	
Commanding General	
U.S. Army Munitons Command	
Attn: Tech. Info. Division	1
Picatinny Arsenal	
Dover, New Jersey 07801	

DISTRIBUTION LIST

Addressee	No. of Copies
Commanding General U.S. Army Munitons Command Attn: AMSMU-LC, CDC Liaison Officer Picatinny Arsenal Dover, New Jersey 07801	1
Commanding General U.S. Army Test & Eval. Command Attn: Tech. Info. Division Aberdeen Proving Ground Maryland 21005	2
Commanding Officer U.S. Army Tank Automotive Center Attn: Research & Dev. Division Mr. V. Pagano Warren, Michigan 48090	1 1
Commanding Officer U.S. Army Research Ofc. - Durham Box CM, Duke Station Attn: Dr. H. M. Davis Durham, North Carolina 27706	1
Commanding Officer Edgewood Arsenal Attn: Director of Products Engrg. Edgewood Arsenal, Maryland 21010	1
Commanding Officer Rock Island Arsenal Attn: Laboratory Rock Island, Illinois 61202	1
Commanding General U.S. Army Engrg. Res. & Dev. Labs. Attn: Mr. W. Baer, SMOFB-SM Fort Belvoir, Virginia	1
Commanding Officer Springfield Armory Attn: Mr. E. H. Abbe, SWESP-RERE Springfield, Mass.	1

DISTRIBUTION LIST

Addressee	No. of Copies
Director U.S. Naval Research Lab. Attn: Code 6340 Washington, D. C. 20025	1
Commandant U.S. Naval Weapons Lab. Attn: Terminal Ballistics Lab Dahlgren, Virginia	1
Commandant U.S. Naval Weapons Lab. Attn: Mr. Rossbacker, Code WC Dahlgren, Virginia	1
Chief, Bureau of Weapons Department of the Navy Washington, D. C. 20025	1
Commander U.S. Naval Engineering Experimental Station Annapolis, Maryland	1
Commander U.S. Naval Engineering Experimental Station Attn: Materials Lab., WCTRL-2 Annapolis, Maryland	1
HQ, Air Research & Development Command Attn: RDRAA Andrews Air Force Base Washington, D. C. 20025	1
Dr. W. Rostoker IIT Research Institute Technology Center 10 W. 35th Street Chicago 16, Illinois	1
Professor J. Wallace Case Institute of Technology Celveland, Ohio	1

DISTRIBUTION LIST

Addressee	No. of Copies
Commanding Officer Watervliet Arsenal Attn: Mr. L. Slawsky, SWEWV-RDR Watervliet, New York	1
Commander U.S. Naval Ordnance Lab. White Oak Silver Spring, Maryland 20910	1
Commander Arnold Engrg. Dev. Center Air Research & Development Center Tullahoma, Tennessee	1
Defense Documentation Center Cameron Station Alexandria, Virginia 22314	20
Chief, Bureau of Ships Department of the Navy Attn: Code 343 Washington 25, D. C.	1
Commanding General Aeronautical Systems Div. Attn: Tech. Info. Division Wright-Patterson Air Base Ohio 45433	1
Commanding General Aeronautical Systems Div. Attn: Aeronautical Research Lab., WCRRL Wright-Patterson Air Base Ohio 45433	1
Mr. Robert H. Brown Aluminum Company of America Alcoa Research Lab. Post Office Box 772 New Kensington, Pennsylvania	1
Professor Merton C. Flemings Massachusetts Institute of Technology Cambridge 39, Massachusetts	1

DISTRIBUTION LIST

Addressee	No. of Copies
Mr. Carson L. Brooks Reynolds Metals Company 4th & Canal Streets Richmond, Virginia	1
Dr. Robert S. Busk Dow Chemical Company Midland, Michigan	1
Dr. Thomas A. Reed University of Illinois Urbana, Illinois	1
Commanding Officer Harry Diamond Laboratories Attn: AMXDO-TIB Washington, D. C. 20438	1
Mr. J. B. Hess Department of Metallurgical Research Kaiser Aluminum & Chemical Corporation Spokane 69, Washington	1
Dr. C. M. Adams Division of Sponsored Research, Room 35-439 Massachusetts Institute of Technology Cambridge 39, Massachusetts	1
Defense Materials Info. Center Battelle Memorial Institute 505 King Avenue Columbus 1, Ohio	1
Commanding Officer Frankford Arsenal Attn: ORDBA-1321 Philadelphia, Pennsylvania	2
Commanding Officer Boston Procurement District Attn: ORDEB-LD Army Base Boston 10, Massachusetts	1
Commanding Officer Frankford Arsenal Attn: SMUFA-1321, Mr. S. Lipson Philadelphia, Pennsylvania	2